

Colors and Mass-to-Light Ratios of Bulges and Disks of Nearby Spiral Galaxies

Akira YOSHINO

*National Astronomical Observatory of Japan,
 Osawa 2-21-1, Mitaka, Tokyo 181-8588
 yoshino.akira@nao.ac.jp*

and

Takashi ICHIKAWA

*Astronomical Institute, Tohoku University,
 Aoba, Sendai, Miyagi 980-8578
 ichikawa@astr.tohoku.ac.jp*

(Received 2004 October 20; accepted 2008 February 15)

Abstract

We investigate colors and mass-to-light ratios (M/L s) of the bulges and disks for 28 nearby spiral galaxies with various morphological types of Sab to Scd, using images in optical and near-infrared (V , I , and J) bands and published rotation curves. It is shown that the observed colors and M/L s generally agree with the galaxy formation model with an exponentially declining star formation rate and shallow slope (ex. Scalo) initial mass function (IMF) for both the bulges and the disks. We find that the bulge M/L is generally higher than the disk M/L and that the galaxies with larger bulge-to-total luminosity ratio tend to have a smaller bulge M/L . The fact indicates that the luminosity-weighted average age of bulges for early-type spirals is younger than that of later-type spirals. These results support a formation scenario that produces young stars for the bulges of middle-type and early-type spirals.

Key words: galaxies: bulges — galaxies: evolution — galaxies: fundamental parameters (colors, mass-to-light ratios) — galaxies: spiral — galaxies: stellar content

1. Introduction

The origin of bulges is a clue to understanding galaxy formation and evolution. Previously two main scenarios: monolithic collapse and secular formation models for the bulge formation have been proposed. In monolithic collapse scenarios, bulges were formed rapidly from primordial gas as well as elliptical galaxies and then disks were grown gradually (e.g., Eggen et al. 1962; Arimoto, Yoshii 1987). On the other hand, in secular formation scenarios, bulges were formed by redistribution or secular heating of disk stars (Zhang 1999), bar dissolution (Kormendy 1979; Norman et al. 1996), or satellite galaxies falling into the host galaxy center region (Aguerri et al. 2001). Thus in these scenarios bulges were formed gradually in disks and consequently do not have uniform age; the average age of some bulges would be as young as that of disks. The bulges formed from secular process are called “pseudo bulges” (e.g., Kormendy, Kennicutt 2004, Laurikainen et al. 2007) in contrast to “classical bulges”, which formed rapidly in high- z . Furthermore, Kauffmann (1996) predicted that the bulges of early-type spirals is younger than the bulges of late-type spirals from her semi-analytic merger models of galaxy formation in a flat cold dark matter universe.

The colors and mass-to-light ratios (M/L s) of bulge and disk are fundamental properties to investigate the origin. In general, both the color index and the M/L

are correlated with the age. However, they are also affected by the metallicity (age-metallicity degeneracy) (e.g., Worthey 1994; Kodama, Arimoto 1997). Moreover, the dust absorption also causes seemingly higher M/L and redder color. Therefore the observations for colors and M/L s in a wide wavelength range are needed to resolve the degeneracy.

Several galaxy formation models predicting the colors and M/L s have been reported. Worthey (1994, hereafter W94) constructed the models with various single starburst-age and the initial mass function (IMF) of Salpeter (1955). He showed that the M/L in I_c band (hereafter we call it simply I band) depends strongly on the age of the system but is nearly independent of the metallicity. Hence he has recommended the use of M/L in the I band to estimate the age of the stellar system.

Bell, de Jong (2001) (hereafter BD01) and recently Portinari, Sommer-Larsen, Tantalo (2004) presented the galaxy evolution models with various e-folding time-scale of star formation rate (SFR) and various IMFs. In the context of their schemes, a shallow slope IMF or a large secondary starburst (e.g., 10% fraction of the total stellar mass) makes M/L smaller than that from single starburst at high- z and steep slope IMF, because the shallow slope IMF reduces the number of low-mass stars, and the large secondary starburst produces the young stars. Comparing the models with the observed disk M/L s of the spiral galaxies in Ursa Major cluster of galaxies, BD01 pointed

out that the observed disk M/L s are generally consistent with the model with shallow slope IMF. However, the bulge M/L s were not explicitly investigated in BD01.

In order to investigate bulge properties, the spiral galaxies should be decomposed into bulge and disk components. Moreover, to obtain bulge M/L s, accurate rotation curves around the galactic center region are necessary. Previously many authors (e.g., Kent 1986; 1987; 1988; Moriondo et al. 1998b) attempted to obtain the colors and M/L s of bulges and disks, and investigated the correlation between M/L s and the dark matter mass, and morphological type of galaxies. The rotation curves used in Kent (1986, 1987, 1988) and Moriondo, Giovanardi, Hunt (1998b) were obtained with HI observations (e.g., Carignan, Freeman 1985; Bosma 1981) or H α observations of Rubin et al. (1985). However, the bulge M/L s may have been underestimated (e.g., Kent 1988; Moriondo et al. 1998b), because the rotation curves used in their analyses may not measure the true circular velocity in the central region of the galaxies. Sofue (1996) claimed that the H α or other ionized gas rotation curves are often influenced by non-circular velocity component (e.g., inflow, outflow or streaming motions) rather than an ordered circular rotation, thus the rotation curve in inner part (≤ 1 kpc) tends to have the slowly rising feature (e.g., Fillmore et al. 1986). Also, since the HI gas cannot be well detected in the region of the central a few kiloparsecs, the rotation velocity was generally smoothed around the central region by observers, the resulting rotation curves have an apparently solid-body (slowly rising) feature (Sofue 1996). Since the M/L is proportional to the square of rotation velocity, the M/L in bulge region is estimated significantly low using the slowly rising rotation curve.

On the other hand, the observation of CO line-emission gives more accurate velocity field at the central region of galaxies because CO molecular gas, which is one of cold interstellar medium, concentrates in the central a few kpc region and is easily detected in the region rather than HI, H α or other ionized gas (Sofue 1996). Therefore the CO rotation curves should represent more accurately the circular rotation velocity and are more desirable to obtain bulge M/L s than other rotation curves. In this paper we use the CO rotation curves of Sofue (1997) and partly Sofue et al. (2003). They observed the CO rotation curves around the centers of nearby galaxies with 45 m telescope at Nobeyama Radio Observatory (NRO) with a resolution of 15 arcsec in Sofue (1997) and Nobeyama Millimeter-wave Array (NMA) with 2-4 arcsec in Sofue et al. (2003), and connected to HI rotation curves for outer regions of galaxies. The resolution of 15 or 2-4 arcsec is not high but enough to discuss bulge properties especially for large nearby galaxies. Indeed, most of the CO rotation curves in Sofue (1997) and Sofue et al. (2003) have revealed steeply rising features, which may be originated from the mass concentration of bulge region, thus the bulge M/L would be higher than previously estimated.

Our motivation in this paper is to evaluate accurately colors and M/L s of bulges and disks and to study the ages. First, galaxy images are decomposed 2-dimensionally into

bulge and disk models. M/L s for bulge and disk are obtained by the fitting of rotation velocity models to the observational ones. In the rotation curve fitting, we adopt “maximum bulge plus disk solution”, which assumes that the inner rotation curve is originated only by the luminous matter. The method is based on van Albada et al. (1985) and Kent (1986). Finally, these results are compared with the stellar population models of W94 and BD01.

In next section, we describe the data and the reductions. The two-dimensional decomposition method for the galaxy images and the fitting method of the velocity model to the rotation velocity data are explained in detail in section 3. We carefully examine the effect of noise and point spread function (PSF) for the images and the aperture effect on the rotation curve measurement on the basis of Monte Carlo simulations with artificial galaxies. In section 4 we show the results for the colors and M/L s of bulge and disk components of the sample galaxies. The results are discussed in section 5 in the context of age and formation of the components. Finally we conclude in section 6.

2. Data and Reductions

2.1. The Sample Galaxies

The sample galaxies are listed in table 1. They are basically taken from Sofue (1997) and Sofue et al. (2003). The galaxies in Sofue (1997) were chosen that (a) the angular size is large enough in order to obtain a sufficiently high linear scale resolution in the central regions; (b) the disk is mildly tilted in order for an accurate correction for the inclination to derive the rotation velocity; (c) no high sensitivity data have been obtained yet with the 45 m telescope or the NMA; and (d) the CO-line emission is sufficiently strong or IRAS 60 and 100 μ m fluxes are higher than several Jy (Sofue 1996). These rotation curves are observed using NRO 45 m with 15 arcsec resolution. Some rotation curves (NGC 4192, NGC 4535, NGC 4536, NGC 4548, and NGC 4569) are taken from Sofue et al. (2003), which targets Virgo cluster galaxies using NMA with 2-4 arcsec resolution. The accuracy of velocity is about $15 - 20$ km s $^{-1}$ for both data of Sofue (1997) and Sofue et al. (2003). We searched for the wide-field imaging data corresponding to the rotation curve data as much as possible. As the result, we obtained the three bands (V , I , and J) imaging data from SMOKA¹ archive system. The numbers of sample are 23 for V band, 24 for I bands, and 20 for J band. The V and I band images were observed with 105 cm Schmidt telescope with a $1k \times 1k$ CCD camera at the Kiso Observatory, University of Tokyo except NGC 3198, NGC 3521, NGC 4258, NGC 4321, NGC 4535, NGC 4536, NGC 4548, NGC 5457, and NGC 7331, which were observed with a $2k \times 2k$ CCD camera. The J band images for 20 galaxies were observed with KONIC (Itoh et al. 1995). The full width half maximum (FWHM)

¹ Based on data collected at Kiso observatory (University of Tokyo) and obtained from data archive at Astronomy Data Center, which are operated by the National Astronomical Observatory of Japan.

of seeing is 3.8 ± 0.9 arcsec for all bands. The exposure time is typically 300s for 1k CCD, 1200s for 2k CCD, and 1800s for KONIC. The information of the telescope and the cameras are listed in table 2.

The data of morphology, isophotal diameter at 25.0 mag arcsec $^{-2}$ in B band (D_{25}) and total magnitude in B band (B_T) in table 1 are taken from “The third reference catalogue of bright galaxies” (RC3) (de Vaucouleurs et al. 1991). The distances for 13 galaxies in table 1 are based on the observation of Cepheid, and those for the remainder are taken from Tully (1988).

Table 2. Specifications of telescope and cameras.

Location	Kiso Observatory
Telescope	105 cm Schmidt Telescope
Camera	1kCCD (TI Japan TC215 1024×1024) 2kCCD (SITe 2048×2048) KONIC (PtSi 1040×1040)
Resolution	0.75 arcsec/pixel (1kCCD) 1.5 arcsec/pixel (2kCCD) 1.06 arcsec/pixel (KONIC)
Field of view	12.5 arcmin×12.5 arcmin (1kCCD) 50 arcmin×50 arcmin (2kCCD) 18 arcmin×18 arcmin (KONIC)

2.2. Reduction and Calibration for Images

The reduction for image data follows standard procedure. We therefore describe only briefly the method. Data analysis were in part carried out on general common use computer system at the Astronomy Data Center, ADC, of the National Astronomical Observatory of Japan. All image reduction is performed with IRAF². Bias and dark counts are subtracted from all images. For the V and I band images, the flat fields are obtained from the median of dome-flat frames. For the J band images, the flat fields are obtained from the median of sky frames acquired before and after the object frames. The object frames are flat-fielded and then sky-subtracted. The field of view of the cameras is large enough to determine the sky background around the galaxies in the image. The sky background counts are estimated on the object frames with SPIRAL package (Ichikawa et al. 1987) installed in IRAF. Finally, the images are rotated to let the major axis of the galaxy horizontal to the bottom. Position angles (PA) taken from RC3 are used to rotate the image for many galaxies. However, we find that the PAs of RC3 are sometimes not suitable for some galaxies from an inspection of model fitting as mentioned in the next section. Therefore we try the following PAs for the galaxy to fit better with the surface brightness model: 0, 30, 60, 90, 120 and 150 degree plus PA of RC3. The best PAs are ascribed in section 4.3.

² IRAF is the Image Analysis and Reduction Facility made available to the astronomical community by the National Optical Astronomy Observatories, which are operated by AURA, Inc., under contract with the U.S. National Science Foundation.

The images are photometrically calibrated with the aperture magnitudes taken from de Vaucouleurs, Longo (1988). Typical photometric errors of the calibration are 0.05 mag for the V and I bands, and 0.08 mag for the J band.

3. Analyses for The Galaxy Images

3.1. Method of Surface Brightness Fitting

First, the galaxy images are decomposed into bulge and disk components. Our decomposition method follows Byun, Freeman (1995). Here the contour of the surface brightness is assumed to be axisymmetric elliptical for both bulge and disk. The centers and the position angles of the bulge and disk are assumed to be common. The 2-dimensional version of generalized model of the surface brightness (Sérsic 1968) is

$$I(r) = I_e \exp[-b_n((r/r_e)^\beta - 1)],$$

$$r = \sqrt{x^2 + (y/(b/a))^2}, \quad (1)$$

where β is the slope of exponent (according to Möllenhoff, Heidt 2001, we use β instead of traditional $1/n$), I_e the effective luminosity in intensity unit, r the radius from the galactic center, r_e the effective radius, b_n a constant relating I_e and r_e (see Moriondo et al. 1998a), x and y distances from the center along major and minor axes, respectively, and b/a the axial ratio. The r of bulge and disk are hereafter denoted as r_b and r_d , respectively. The b/a of bulge and disk are hereafter denoted as $(b/a)_b$ and $(b/a)_d$, respectively. μ_e in mag arcsec $^{-2}$ is also used instead of the I_e . For disk, we assume $\beta=1$ (exponential law) (Freeman 1970). Thus the surface brightness of disk is

$$I_d(r) = I_0 \exp[-(r_d/r_h)],$$

$$r_d = \sqrt{x^2 + (y/(b/a)_d)^2}, \quad (2)$$

where I_0 and r_h are the central luminosity and the scale length, respectively. μ_0 in mag arcsec $^{-2}$ is also used instead of the I_0 .

For bulge, various values of the slope $\beta = 1/n$ have been reported (e.g., Caon et al. 1993; Andredakis, Sanders 1994; Andredakis et al. 1995; de Jong 1996a; Seigar, James 1998; Moriondo et al. 1998a; Möllenhoff, Heidt 2001). In general, β has thought to be within the range of 1 (exponential law) to 1/4 (de Vaucouleurs' law) (de Vaucouleurs 1953). For $\beta = 1$,

$$I(r) = I_e \exp[-1.68((r_b/r_e)^\beta - 1)],$$

$$r_b = \sqrt{x^2 + (y/(b/a)_b)^2}, \quad (3)$$

For $\beta = 1/4$, it is

$$I(r) = I_e \exp[-7.67((r_b/r_e)^\beta - 1)]. \quad (4)$$

If the β is the free parameter in the decomposition, it is not generally well determined, because the point spread function (PSF) and the disk parameters may affect the estimating β (e.g., de Jong 1996a; Moriondo et al. 1998a; Balcells et al. 2003). de Jong (1996a) and other recent

Table 1. The list of the galaxies.

Name (1)	Type (2)	Distance (3)	D_{25} (4)	B_T (5)	Band (6)	RC (7)
NGC 253	SAB(s)c	3.0 ⁽¹⁾	27.5	8.04	V, I, J	1
NGC 891	SA(s)b:	9.6 ⁽¹⁾	13.5	10.81	V, I, J	1
NGC 1068	RSA(rs)b	14.4 ⁽¹⁾	7.1	9.61	V, I	1
NGC 1808	RSAB(s)a	10.8 ⁽¹⁾	6.5	10.76	J	1
NGC 2403	SAB(s)cd	3.2 ⁽²⁾	21.9	8.93	V, I	1
NGC 2841	SA(r)b:	14.1 ⁽³⁾	8.1	10.09	V, I, J	1
NGC 2903	SAB(rs)bc	6.3 ⁽¹⁾	12.6	9.68	V, I, J	1
NGC 3031	SA(s)ab	3.63 ⁽⁴⁾	26.9	7.89	V, I, J	1
NGC 3079	SB(s)c	20.4 ⁽¹⁾	7.9	11.54	V, I, J	1
NGC 3198	SB(rs)c	14.5 ⁽⁵⁾	8.5	10.87	V, I, J	1
NGC 3521	SAB(rs)bc	7.2 ⁽¹⁾	11.0	9.83	V, I, J	1
NGC 3628	SAb pec	7.7 ⁽¹⁾	14.8	10.28	J	1
NGC 4192	SAB(s)ab	16.1 ⁽⁶⁾	9.8	10.95	V, I	2
NGC 4258	SAB(s)bc	7.8 ⁽⁷⁾	18.6	9.10	V, I, J	1
NGC 4303	SAB(rs)bc	15.2 ⁽¹⁾	6.5	10.18	J	1
NGC 4321	SAB(s)bc	16.1 ⁽⁶⁾	7.4	10.05	V, I, J	1
NGC 4535	SAB(s)c	16.1 ⁽⁶⁾	7.1	10.59	V, I, J	2
NGC 4536	SAB(rs)bc	16.1 ⁽⁶⁾	7.6	11.16	V, I, J	2
NGC 4548	SB(rs)b	16.1 ⁽⁶⁾	5.4	10.96	V, I	2
NGC 4565	SA(s)b:	9.7 ⁽¹⁾	15.9	10.42	V, I	1
NGC 4569	SAB(rs)ab	16.1 ⁽⁶⁾	9.5	10.26	V, I	2
NGC 4631	SB(s)d	6.9 ⁽¹⁾	15.5	9.75	J	1
NGC 4736	RSA(r)ab	4.3 ⁽¹⁾	11.2	8.99	I, J	1
NGC 5194	SA(s)bc pec	7.7 ⁽¹⁾	11.2	8.96	V, I	1
NGC 5457	SAB(rs)cd	7.4 ⁽⁸⁾	28.8	8.31	V, I	1
NGC 5907	SA(s)c:	14.9 ⁽¹⁾	12.8	11.12	V, I, J	1
NGC 6946	SAB(rs)cd	5.5 ⁽¹⁾	11.5	9.61	V, I, J	1
NGC 7331	SA(s)b	15.1 ⁽⁹⁾	10.5	10.35	V, I, J	1

Col.(1) : NGC Number. Col.(2) : Type taken from RC3.

Col.(3) : Distance [Mpc]. ⁽¹⁾ Tully (1988) ⁽²⁾ Freedman, Madore (1988)⁽³⁾ Macri et al. (2001) ⁽⁴⁾ Freedman et al. (1994) ⁽⁵⁾ Kelson et al. (1999)⁽⁶⁾ Ferrarese et al. (1996) ⁽⁷⁾ Newman et al. (2001) ⁽⁸⁾ Kelson et al. (1996)⁽⁹⁾ Hughes et al. (1998)

Col.(4) : Diameter taken from RC3 [arcmin]. Col.(5) : Total magnitude taken from RC3 [mag].

Col.(6) : Band for imaging. Col.(7) : Reference of the Rotation Curve. 1 is Sofue (1997),

2 is Sofue et al. (2003).

studies claimed that about more than fifty percent bulges in nearby galaxies are fitted with exponential law rather than de Vaucouleurs' law. We therefore fixed the value of β . At first we try $\beta = 1/4, 1/3, 1/2$, and 1. We find that the fitted value of β is 1 or $1/2$ for most of our sample galaxies. Then we add $\beta = 2/3 = 0.67$ and $\beta = 3/4 = 0.75$ models to examine carefully the bulge shape between $\beta = 1/2$ and $\beta = 1$. As the results, some galaxies (NGC 3198, 3521, 4258, 4548, 4736, 5907 and 6946) are well fitted using the $\beta = 2/3$ or $\beta = 3/4$ bulge models rather than the $\beta = 1/2$ or $\beta = 1$.

NGC 1068, 1808, 2841, 3031, 3079, 4192, 4258, 4303, 4548, 4565, 4569 and 5194 are classified as Seyfert galaxies. Some other galaxies also have a bright central point source, however they are not classified as Active Galactic Nuclei (AGN). Hence the nuclear parameters (central lu-

minosity of the point source I_{nuc} , or M_{nuc} in magnitude unit) are added into the bulge/disk decomposition program. The total surface brightness of a galaxy is sum of I_b , I_d and I_{nuc} . In practice, the extra luminosity I_{nuc} turns out to be negative value for some galaxies. When the nucleus luminosity is negative, the galaxy is fitted with only bulge and disk parameters. To simplify, spiral arms, bar and ring structures are not included in our model.

The observed images are convolved with seeing and instrument point spread function (PSF). Hence it is required that the observed images are deconvolved with the PSF or the model images are convolved. However, the deconvolution may add the artificial noise and may change the profile of the galaxy (especially for bulge). Therefore, instead of the deconvolution for the observed image, we convolved the model surface brightness.

In general, the higher signal-to-noise ratio (S/N) and the larger number of pixels give the better analysis. The distances of x and y from the galactic center having $S/N > 10$ are measured and the pixels within the rectangle are used in the analysis. We found empirically that this method gives better fitting.

To obtain the parameters, chi-square (χ^2) is defined as

$$\chi^2 = \sum_i \frac{(I_{obs}(x, y) - I_m(x, y))^2}{\sigma_i^2}, \quad (5)$$

where $I_{obs}(x, y)$ is the observed value of the galaxy surface brightness, and $I_m(x, y) = I_b(x, y) + I_d(x, y) + I_{nuc}(x, y)$ is convolved with Moffat function (Moffat 1969),

$$PSF(r) = (\beta - 1)[1 + (r/\alpha)^2]^{-\beta} / \pi\alpha^2, \quad (6)$$

$$FWHM = 2\alpha\sqrt{2^{1/\beta} - 1}, \quad (7)$$

where FWHM and β (this is not the bulge slope) are taken from the average values for those of a few stars in the frame calculated from the “imexam” task of IRAF. Being assumed Poisson distribution, the uncertainty (σ_i) is set to the square root of $(I_{obs}(x, y) + I_{sky}(x, y) + (I_{read}/\alpha)^2)/\alpha$, where I_{sky} is the sky level, I_{read} the read noise, and α the conversion factor. We confirm that this σ_i gives the smallest scattering in the comparison of input-output parameters for our simulated images as discussed in section 3.2. The parameters in the model are obtained by a nonlinear least square fitting, which minimizes the χ^2 . Our calculation is based on Marquardt method (Press et al. 1988). Various models including $\beta = 1/n$ and PA are tried for each galaxy, and the best model that χ^2 is the smaller than other models is found.

Although the χ^2 is useful to find the better model for one galaxy, they are not useful to compare the error of fitting between sample galaxies, because the χ^2 may become large or small due to the adopted weighting factor $1/\sigma_i^2$, as Baggett, Baggett, Anderson (1998) have pointed out. To compare the error of fitting between galaxies, we calculate the total residual ($\sqrt{\sum_i (I_{obs}(x, y) - I_m(x, y))^2}$) in magnitude unit. They are tabulated in table 3-5 and are about 0.1-0.3 mag.

We next correct the obtained bulge μ_e and disk μ_0 with the Galactic extinction. The extinction is taken from the table of NED (NASA/IPAC Extragalactic Database)³, which is calculated from the data of Schlegel, Finkbeiner, Davis (1998). The total model magnitudes of bulge, disk and the total galaxy (bulge + disk + nucleus) are calculated by integrating the model surface brightness of each component from center to infinity for each band. The colors of bulge and disk are calculated from the model magnitudes of V , I and J bands.

3.2. Accuracy of The Surface Brightness Fitting

We construct model images and then decompose them to examine how well the parameters are reproduced by

our analysis. We make 300 models for each $\beta = 1/4$ (de Vaucouleurs), $1/3$, $1/2$, $2/3$, $3/4$, and 1 (exponential) bulge + exponential disk + nucleus. The values of the six parameters are selected at random. Three parameters are set to the following range: $0.3 < (b/a)_b < 1.0$, $0.1 < (b/a)_d < 0.8$ and $30 < r_h < 150$ arcsec. Also the disk μ_0 are set to $18 < \mu_{0,V} < 22$, $17 < \mu_{0,I} < 21$, and $16 < \mu_{0,J} < 20$ mag arcsec⁻² for V , I , J band, respectively. Also the nuclear magnitude M_{nuc} are set to $12 < M_{nuc,V} < 16$, $11 < M_{nuc,I} < 15$, and $10 < M_{nuc,J} < 14$ mag arcsec⁻² for V , I , J band, respectively.

Since μ_e and r_e are inversely proportional to the slope β (cf., de Jong 1996a; Moriondo et al. 1998a), the model μ_e and r_e should be set to suitable ranges for the assumed β . To simplify, μ_e and r_e for $\beta = 1/4$ and $\beta = 1/3$ are set to $19 < \mu_{e,V} < 23$, $18 < \mu_{e,I} < 22$, $17 < \mu_{e,J} < 21$ mag arcsec⁻² and $10 < r_e < 100$ arcsec, while those for $\beta = 1/2$, $2/3$, $3/4$, and 1 are set to $18 < \mu_{e,V} < 22$, $17 < \mu_{e,I} < 21$, $16 < \mu_{e,J} < 20$ mag arcsec⁻² and $5 < r_e < 50$ arcsec. Those parameter ranges are typical in our sample galaxies.

Here we show the results using the instrument features of 1kCCD and KONIC. The results for 2kCCD camera are almost the same as for 1kCCD. To simulate the images observed with 1kCCD camera or KONIC, the exposure times are set to 300s for V and I band and 1800s for J band. The specifications of 1kCCD camera for V and I bands and those of KONIC for J band are input to the model images. The V and I band images are convolved with Moffat function. The FWHM is assumed to be 3.8 arcsec, and the parameter β is set to 4.0, which are average values in our galaxies. The J band images are convolved with a special PSF for KONIC⁴. Then, the background noise according to the exposure time and the performance of the detectors are added to the convolved images. Finally those simulated image is decomposed into bulge, disk and nucleus to obtain the seven parameters. Then the input parameters are compared with the outputs.

From figures 1-4, we can look how well the parameters are reproduced. Here we show the results of $\beta = 1$ and $\beta = 1/4$ for V band (figure 1-2), $\beta = 1$ for I band (figure 3), and $\beta = 1$ for J band (figure 4). Figure 1-3 indicate that the simulated images are fitted with the models in high accuracy. Other models ($\beta = 1/3, 1/2, 2/3, 3/4$) are also well fitted, however they are not illustrated. We find that the 1σ errors of all parameters for the V and I band images are less than 1% of the original values expect for the M_{nuc} at the $\beta = 1/4$ models. On the other hand, the errors are relatively large in the J band (figure 4). The large amount of background noise should cause the fitting error for J band. However the scattering is relatively small within a limited range of parameter values; $0.01 < B/T < 0.4$ and $\mu_{0,J} < 18$, which is denoted as black circles in figure 4. Therefore we only use the fitting results within the permitted range. The 1σ errors in the range for the J band are 0.17 mag, 0.06, 5.7 arcsec, 0.16 mag, 0.02, 5.0 arcsec, 0.01 mag for bulge μ_e , $(b/a)_b$, r_e , disk μ_0 , $(b/a)_d$,

³ The NASA/IPAC Extragalactic Database (NED) is operated by Jet Propulsion Laboratory, California Institute of Technology, under contract with the U.S. National Aeronautics and Space Administration.

⁴ The data is available at <http://www.ioa.s.u-tokyo.ac.jp/kisohp/INSTRUMENTS/konic/psf2.gif>.

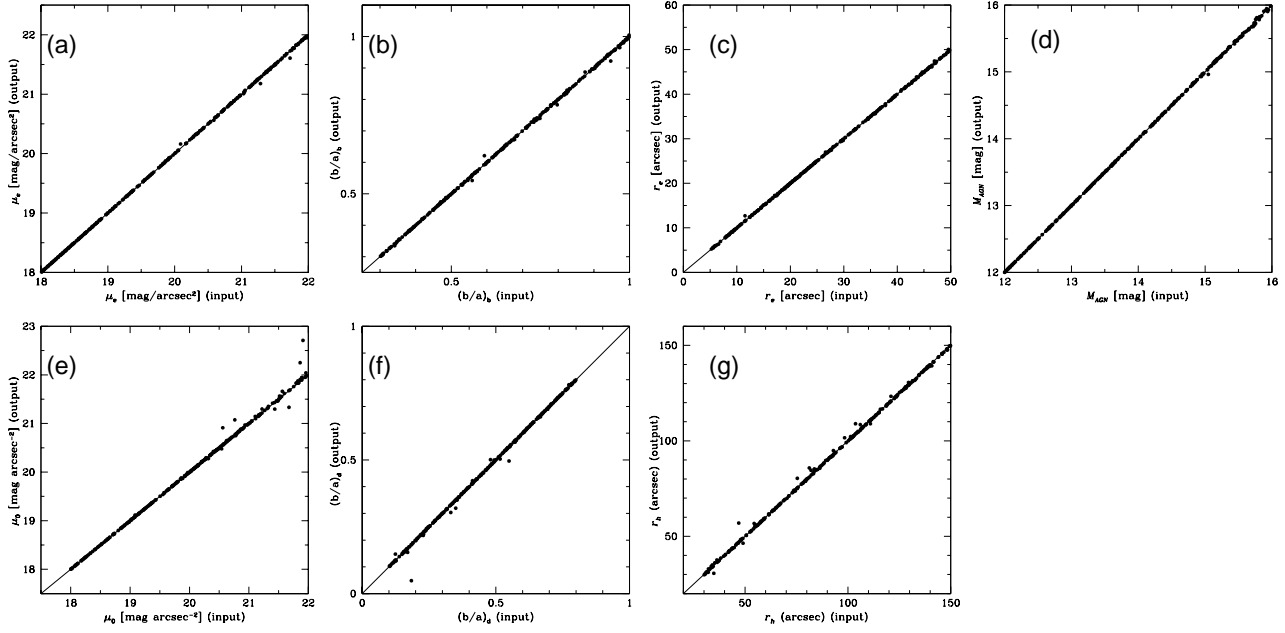


Fig. 1. The result of the two-dimensional decomposition with artificial galaxies for $\beta = 1$ bulge model and V band. The solid lines in each panel show the equality of input and output parameters. (a) bulge effective luminosity μ_e . (b) bulge axial ratio $(b/a)_b$. (c) bulge effective radius r_e . (d) Nucleus magnitude M_{nuc} . (e) disk central luminosity μ_0 . (f) disk axial ratio $(b/a)_d$. (g) disk scale length r_h .

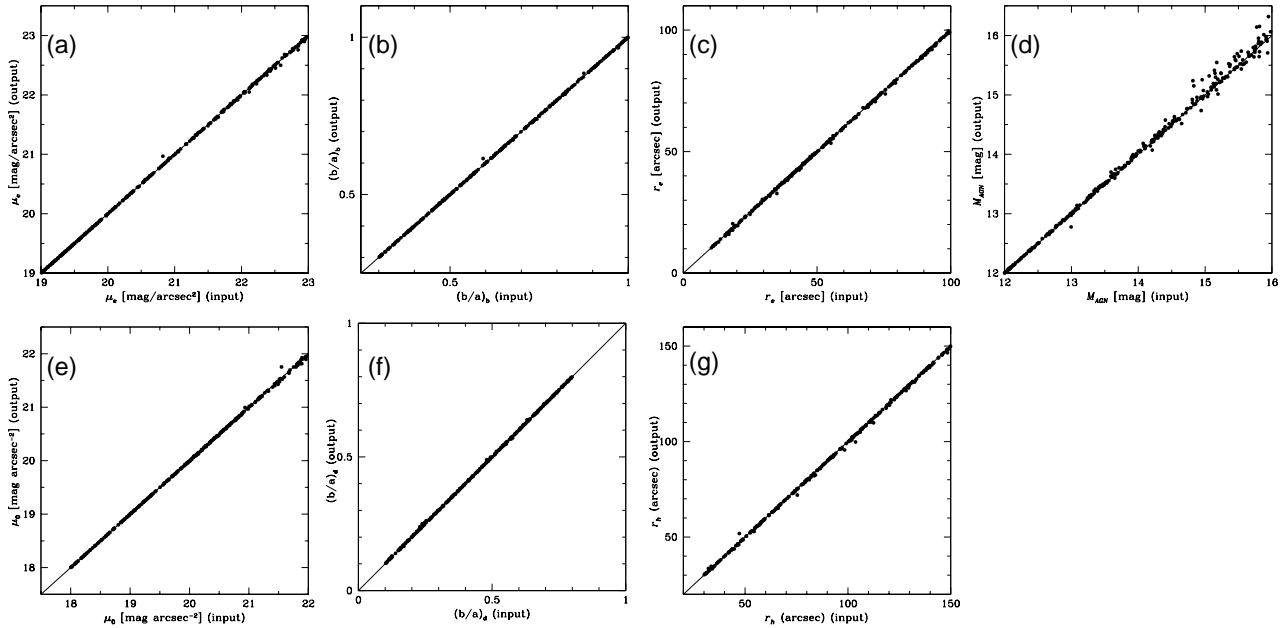


Fig. 2. The same as for figure 1, but for $\beta = 1/4$ bulge model and V band.

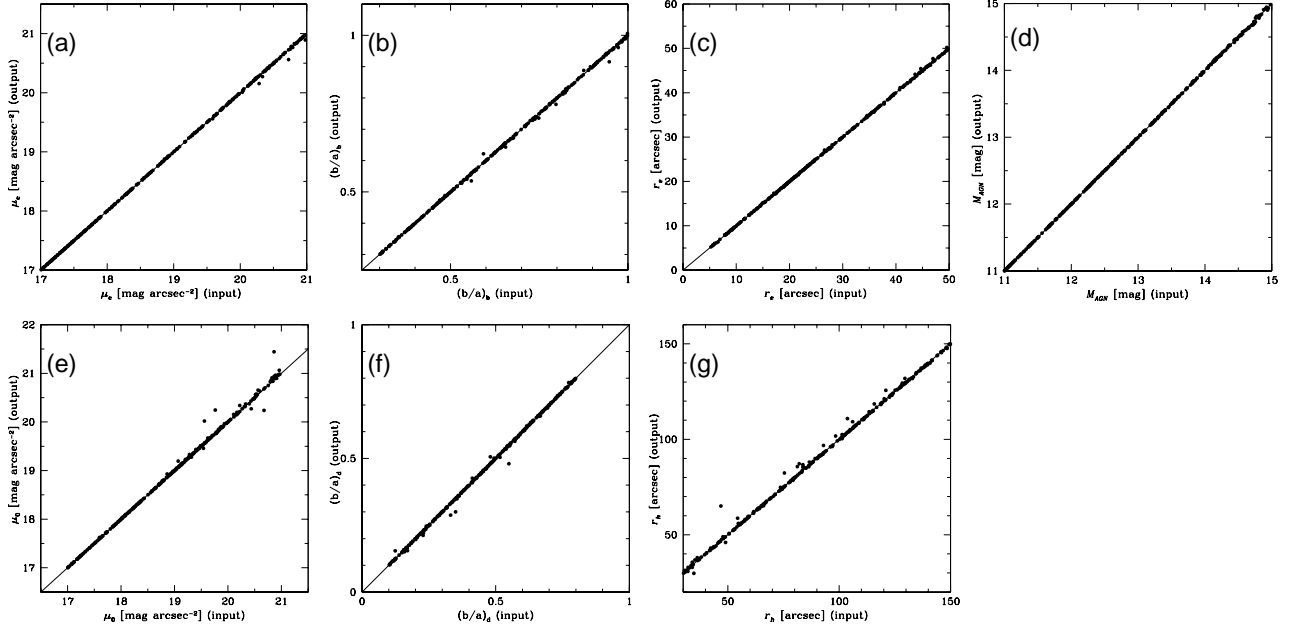


Fig. 3. The same as for figure 1, but for I band.

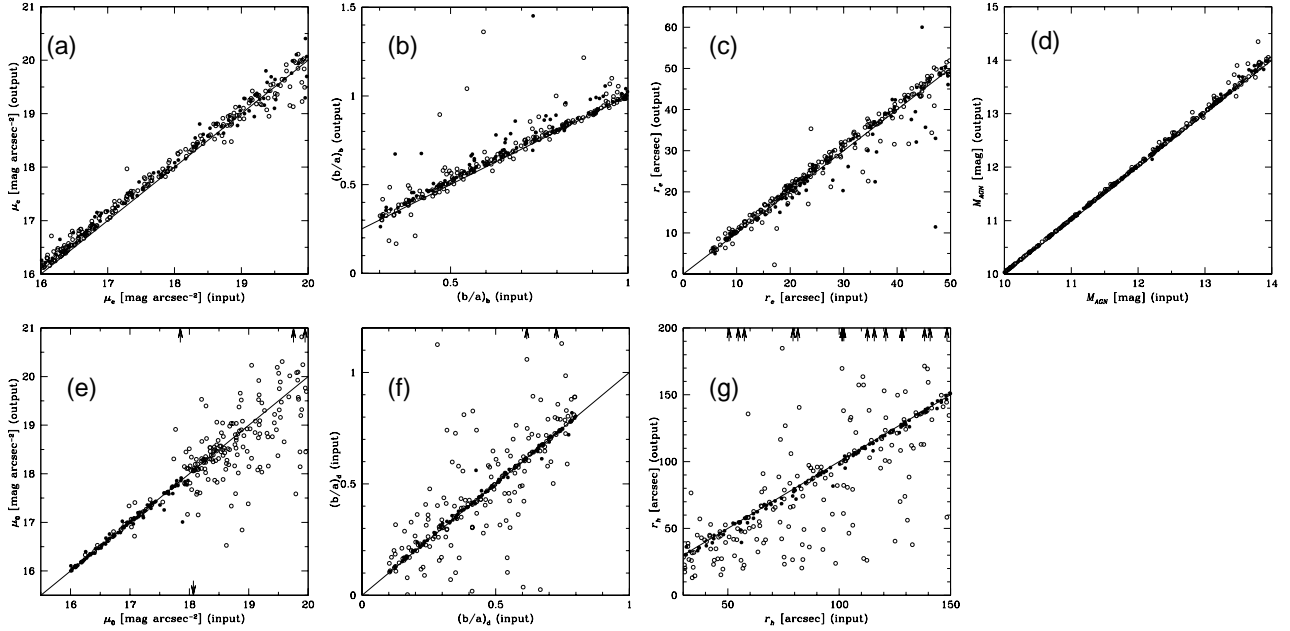


Fig. 4. The same as for figure 1, but for J band. The filled and open circles denote the models within the range of $0.01 < B/T < 0.4$ and $\mu_{0,J} < 18.0$ and the models outside the range, respectively. The arrow shows the data located outside the figure.

r_h , and M_{nuc} , respectively.

3.3. Model of Rotation Curve

After the surface brightness decomposition of the galaxies images, the rotation curves of Sofue (1997) and Sofue et al. (2003) are decomposed into the contribution from the bulge, disk and halo component to obtain those M/L s. On the assumption of the constant M/L , the mass surface density distribution $M(r)$ for bulge or disk component is expressed as

$$M(r) = (M/L) \times I(r), \quad (8)$$

where $I(r)$ is the luminosity density for bulge or disk in solar luminosity unit. The unit of M/L is $(M/L)_\odot$ (ratio of solar mass to solar luminosity).

The circular velocity for ellipsoidal bulge is given by (Binney, Tremaine 1987):

$$v_b^2(r) = 4\pi G(M/L)_b \sqrt{1 - \epsilon^2} \int_0^r \frac{j_b(a) a^2 da}{\sqrt{r^2 - a^2 \epsilon^2}}, \quad (9)$$

where $(M/L)_b$ the bulge M/L , $j_b(a)$ the luminosity density at distance a from the center in the equatorial plane, and $\epsilon = \sqrt{1 - b^2/a^2}$ the constant intrinsic eccentricity. To obtain the $j_b(a)$, we consider the “strip brightness” $S(a)$, defined as the integral of the bulge brightness distribution along a path orthogonal to the line of nodes, at distance a from the center (Moriondo et al. 1998b). Then

$$\frac{dS}{da} = -2\pi \sqrt{1 - \epsilon^2} a j_b(a). \quad (10)$$

On the other hand, the circular velocity for exponential disk is given by (Freeman 1970):

$$v_d^2(r) = 4\pi G \Sigma(0) r_h y^2 [I_0(y) K_0(y) - I_1(y) K_1(y)], \quad (11)$$

where $y = r/2r_h$, $I_n(y)$ and $K_n(y)$ are the modified Bessel functions of first and second kind, respectively, $\Sigma(0) = (M/L)_d I_0$ the central disk surface density, and $(M/L)_d$ the disk M/L .

The mass of the nucleus is about $10^7 M_\odot$ for NGC 1068 (Greenhill et al. 1996) and generally smaller than $10^6 - 10^7 M_\odot$ for other spirals (Salucci et al. 2000), which influence hardly the rotation curves at least the 15 or 2-4 arcsec resolution of Sofue (1997) or Sofue et al. (2003) rotation curves. Therefore the contribution of nucleus on rotation curve is ignored in this paper.

The observed rotation curves may be superposed by non-circular motions induced by bar. The bar-influenced gas flow at a side-on view gives lower rotation velocity, whereas that at an end-on view give higher rotation velocity (Sofue 1997). If the effect of bar-influenced gas flow is large, most of rotation curves will indicate lower and more gradually rising features, because the probability of looking bar at an end-on view is lower than that at an side-on view (Sofue 1997). However, Sofue (1997) reported that most of rotation curves have the steep rise features and there are no significant difference in the rotation curves between the barred galaxies and the normal spiral galaxies. Hence the steep rise feature should be due to mass concentration within the bulge at zero-th order

approximation (Sofue 1997). Therefore the effects of bar is ignored.

There is a massive dark matter (halo) in galaxies. The halo produces flat or nearly flat rotation curves in most galaxies (e.g., Barnaby, Thronson 1994). The pseudo-isothermal sphere model possesses this property, and its density distribution is given by (Kent 1986):

$$\rho(r) = \rho_{0,h} / [1 + (r/R_h)^2] = \sigma_h / [2\pi G(r^2 + R_h^2)], \quad (12)$$

where $\rho_{0,h}$ the halo’s central mass density, R_h the halo core radius, and σ_h the velocity dispersion. This distribution gives the rotation curve of

$$v_h(r)^2 = 2\sigma_h^2 [1 - (R_h/r) \tan^{-1}(r/R_h)]. \quad (13)$$

The dark halo parameters are strongly affected by the observed maximum radius of rotation curve. In this paper we consider mainly M/L of luminous matter, thus the discussion in the reliability of halo parameters is beyond our scope. The influence of dark halo blending on the maximum bulge plus disk solutions is discussed in the next section.

The gravitational potential, ϕ , of a spiral galaxy is a superposition of the potentials generated by its individual mass components (Kent 1986; Barnaby, Thronson 1994),

$$\phi = \phi_b + \phi_d + \phi_h. \quad (14)$$

Thus we get an expression for the model rotation velocity

$$v(r)^2 = v_b(r)^2 + v_d(r)^2 + v_h(r)^2. \quad (15)$$

We use again Marquardt method to fit rotation curves. Here the uncertainty of observed rotation curve is set to constant over the full range, because the error size of the observed rotation curve is nearly constant from the center to the end. We input the uncertainty of $15 [\text{km s}^{-1}]/\sin i$ (Sofue 1997; Sofue et al. 2003) to rotation curve fitting, where i is the inclination of the galaxy. The i are calculated with $i = \cos^{-1}(1/R_{25})$, where R_{25} are axial ratios taken from RC3.

The parameters used in the rotation curve fitting are $(M/L)_b$, $(M/L)_d$, σ_h , and R_h . The solution of these four parameters obtained simultaneously is called “full solution”. However, in practice, the full solution is often singular because the observed rotation curves do not extend far enough to decouple the interdependence of the disk M/L ratio and halo parameters (Kent 1986). Hence van Albada et al. (1985) and Kent (1986) devised the method restricting parameters and obtaining the solutions step by step. The solutions obtained with the method is called “maximum bulge plus disk solution” or “maximum disk solution”. We also adopt the method in our analysis. In this method we assume that rotation curve can be fitted by only visible matter within the radius of two times of disk scale length (r_h), which gives maximum v_d and thus maximum $(M/L)_d$. Thus two parameters ($(M/L)_b$ and $(M/L)_d$) are determined within $2r_h$. Next, holding the resulting values, we obtain the remaining parameters (σ_h and R_h) by fitting the full range of rotation curve.

If the observed rotation curve has the slowly rising feature compared to the luminosity concentration of bulge and is well fitted by only disk contribution, the $(M/L)_b$ tends to be nearly zero or negative. In fact, we obtain negative $(M/L)_b$ for NGC 3198 in the I band. The effect of beam smearing of rotation curve would cause the slowly rising feature. Since the negative values of M/L s are nonsense, we restrict the parameters to positive in the fitting.

3.4. Accuracy of The Rotation Curve Fitting

In order to examine an accuracy of the rotation curve fitting, we construct 300 model rotation curves and then apply our method to the models. The distances are set to 10 Mpc. The radii of the rotation curves are fixed to 500 arcsec, which corresponds to 24 kpc at the distance of 10 Mpc. These are the typical observations of Sofue (1997). We select the parameters at random within the following range: $0.5 < (M/L)_b < 3.0$, $0.5 < (M/L)_d < 3.0$, $100 < \sigma_h < 150 \text{ km s}^{-1}$, $100 < R_h < 500 \text{ arcsec}$. The ranges of luminosity parameters (μ_e , μ_0 and so on for each β , V , I and J) input in the simulation are the same as above section. The ranges of $(M/L)_b$, $(M/L)_d$, σ_h and R_h are taken from the typical values in Kent (1986). Here we show the result with the μ_e and μ_0 for $\beta = 1$ and I band. Other cases of β or bands are also tried, and the similar results are obtained. Using these parameters, the dark-to-luminous (bulge + disk) mass ratio of model galaxy is within the range of 0.07 (luminous matter dominating) to 32.2 (dark matter dominating) (typically about 3), and the total M/L_I ratio of the galaxy is within the range of 1.0 to 69.1 (typically about 6). These values are generally consistent with those of previous authors (e.g., Kent 1986, 1987).

The rotation curves in Sofue (1997) and Sofue et al. (2003) were observed with the angular resolution of 15 arcsec and 2-4 arcsec, respectively. Hence the model rotation curves are convolved with Gaussian with FWHM of 15 arcsec or 3 arcsec. Here we show the result of the case of 15 arcsec resolution. Finally the simulated rotation curves are fitted to the velocity model with the maximum bulge and disk method.

The radius from the galactic center used in the maximum disk method affects the accuracy of fitting. In general, a large radius would bring a contamination of dark halo, while a small radius would bring a confusion of bulge and disk. Thus we examine radii of 1, 2 and 3 times of disk r_h . We confirm that 2 r_h , which was used also in Moriondo, Giovanardi, Hunt (1998b), gives the best fitting. Therefore we adopt 2 r_h in the following discussion.

Figure 5 shows the comparisons of the relative residuals ((output-input)/input) with μ_e or μ_0 . The systematic error for bulge M/L against μ_e and disk M/L against μ_0 are clearly seen in the figure. The bulge error is mainly caused by the disk contamination, while the disk error is mainly caused by the dark halo contamination. We find empirically that the errors are relatively small for the range of $\mu_{e,I} < 19.5$, $\mu_{0,I} < 19.5$ ($\mu_{e,V} < 20.5$, $\mu_{0,V} < 20.5$ for V band, $\mu_{e,J} < 18.5$, $\mu_{0,J} < 18.5$ for J band), and

$0.01 < B/T < 0.5$. We therefore reject the results outside the above ranges. For about 6 % of the models, the output values of M/L s are smaller than 0.1, which are clearly out of the range predicted from galaxy formation models. Therefore we adopt only the models of output $M/L > 0.1$ for estimating the error of M/L . Using the result of the examination, we correct the fitting results of bulge and disk M/L s for sample galaxies according to μ_e and μ_0 , respectively. The correction of systematic error of M/L s for bulge and disk are not considerably large within the reliable parameter ranges: about factor of 1.0-1.3 and 0.9-1.0 of originally obtained values, respectively. The scatterings of bulge and disk M/L s within the ranges in our simulation are about 10-15% and 6-8%, respectively. In practice, since the errors of surface brightness parameters and the residual χ^2 are added, the errors of M/L for observed galaxies are somewhat enlarged; about 15-30% for both of bulge and disk M/L .

4. Results

4.1. Fitting Result of Surface Brightness and Rotation Curves

Figure 6 shows the luminosity profiles and rotation curves of sample galaxies. The results of fittings for surface brightness and rotation curve are listed in tables 3-5 and 7-9, respectively.

The surface brightness parameters for NGC 1808 (J) and 4536 (J) are not obtained because of poor weather condition. The edge-on galaxy NGC 891 is also not well fitted to any model in all bands because of the dust lane. The parameters for NGC 4321 and 4535 in the J band are unreliable, because they are dimmer than the reliable range of disk central luminosity $\mu_{0,J}$. The parameters for NGC 2903, 3198, 4258 and 4736 in the J band may be also unreliable, because the image quality (S/N) are relatively low and the values of r_e or r_h in the J band for these galaxies are considerably different from those of V and I band. We exclude these data in the discussion. The image of nucleus region for NGC 4736 (I) is saturated, hence the parameters may be somewhat inaccurate, however the residual of fitting is small. The results of surface brightness fitting for 22 (V), 23 (I) and 10 (J) galaxies are reliable and are used in the discussion of the structural parameter, color and magnitude.

The χ^2 values in the surface brightness fitting turn out to be almost the same among various $\beta = 1/n$ models of bulge. Thus the β is not well determined only by the surface brightness. However, the χ^2 value in the rotation curve fitting clearly depends on β , because the central rising and peak of rotation curve is sensitive to the bulge β . Consequently we obtain the β by the result of rotation curve fitting. In fact, the central rising part of rotation curve observed in Sofue (1997) and Sofue et al. (2003) are well reproduced by the exponential bulge in many galaxies. The fact that the $\beta \geq 1/2$ model is more suitable than $\beta < 1/2$ model has been reported by other authors (e.g., de Jong 1996b, Möllenhoff, Heidt 2001, Graham 2001, MacArthur, Courteau 2003, Hunt et al. 2004). Our re-

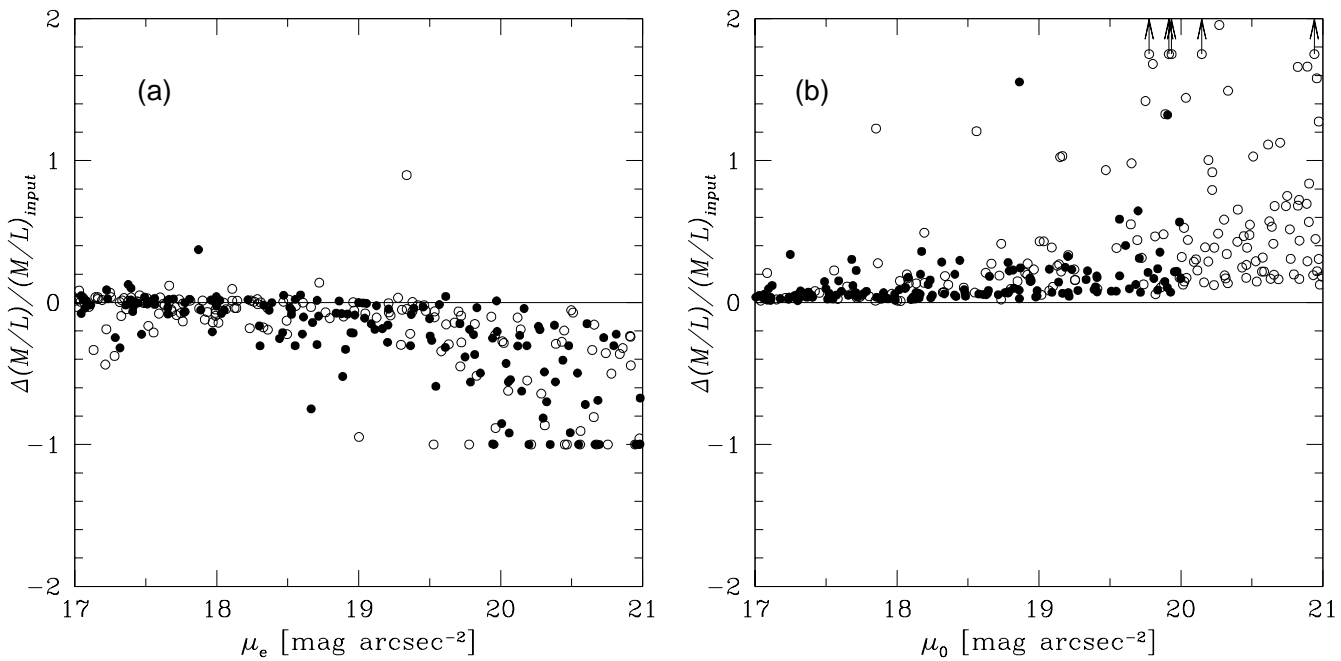


Fig. 5. The result of the rotation curve decomposition with artificial galaxies for I band. (a) : The comparison of the relative residuals $((\text{output}-\text{input})/\text{input})$ of bulge M/L versus μ_e . The filled and open circles denote the models within the range of $0.01 < B/T < 0.5$ and $\mu_{0,I} < 20$ and the models outside the range, respectively. (b) : The same as (a), but for disk M/L versus μ_0 .

sults agree with these recent studies.

When bulge μ_e and/or disk μ_0 are larger (fainter) than the reliable ranges, the M/L s of bulge or disk are also unreliable. Furthermore, the bulge M/L (and color) in the galaxy of inclination $i > 75$ degree would be influenced by dust extinction and thus unreliable, as mentioned in section 4.4. These data are denoted as colon in the tables 7-9. The bulge M/L for 13 (V), 14 (I) and 5 (J) galaxies and the disk M/L for 17 (V), 21 (I) and 11 (J) galaxies are reliable and are used in the discussion.

Indeed, the rotation curves are not perfectly fitted with the model, especially for the inner region of NGC 1068, NGC 2841, NGC 3031, NGC 4548 and NGC 4569. There would be some reasons for the discrepancy. One reason may be the gravitation of massive components (e.g., inner bar and ring) other than bulge and disk around the galactic center. It would be appropriate for NGC 1068 and NGC 4548; the former has a ring and another complex structure in the inner region (RSA(rs)b), and the latter is classified as the barred galaxy (SB(rs)b). Another reason would be the low resolution of 15 arcsec for CO rotation curves. It may be valid partly for NGC 1068, NGC 2841 and NGC 3031. The reason of discrepancy for NGC 4569 rotation curve around the galactic center, of which resolution is 4 arcsec (Sofue et al. 2003), remains unknown in this paper. The more careful and complex method of model fitting for rotation curve should be studied in the future.

The halo parameters are significantly affected by the observed radius of rotation curve from the galactic center

(cf. Kent 1986; Moriondo, Giovanardi, Hunt 1998b). If the radius does not extend far enough to decompose into luminous matter and dark matter, the rotation curve can be fitted with only bulge and disk, and the halo parameters are not well determined. In fact, the halo parameters for some galaxies are not determined or implausible. Since we focus on only M/L s for bulges and disks in this paper, the halo parameters are not used in the following discussion.

4.2. The Trend of Bulge and Disk Scale Parameters

We compare the scale length and bulge effective radius in three bands to check the validity of the fitting. Figure 7 and 8 show the trend of r_e and r_h on the bands, respectively. The values are normalized for those of V band. Only 13 galaxies (NGC 253, 2841, 2903, 3031, 3079, 3198, 3521, 4258, 4321, 4535, 5907, 6946 and 7331) are decomposed for all (V , I , J) bands and plotted in the figures. Those of J band for NGC 2903, 3198, 4258, 4321 and 4535 are unreliable as described in the previous section and are connected by dashed lines in the figures. There is no significant trend between the bulge effective radius r_e and the band in figure 7, while MacArthur, Courteau (2003) reported that r_e increases with longer wavelength band, however the scattering is large. On the other hand, the disk scale length r_h generally decreases from V to J in figure 8. The trend has been reported in Möllenhoff (2004). The decreasing r_h toward the redder bands would be caused by the higher concentration of old stars in the central region and/or an increasing of star for-

mation in the outer disk (e.g., MacArthur, Courteau 2003; Möllenhoff 2004). More sample is necessary to discuss the correlation.

4.3. The Position Angles and Axial Ratios

To simplify, the PA of galaxy is not the fitting parameter but is fixed to 0, 30, 60, 90, 120 and 150 degree plus the RC3 data in this paper. Each galaxy image rotated with these PAs is fitted with the surface brightness model to decide the best PA from the smallest χ^2 . As the result, the PAs for many galaxies are 0 plus RC3's PA. That is to say, the RC3 data are suitable. The PAs for some nearly face-on galaxies do not agree with RC3 data, however. We adopt the following PAs for some galaxies: RC3's PA plus 30 degrees for NGC 1068, plus 60 degree for NGC 4303, plus 90 degrees for NGC 4321 and NGC 4548, 120 degrees for NGC 5194 and 60 degrees for NGC 6946. The discrepancy of obtained PA between our analysis and RC3 for some face-on galaxies would be due to the following reason: The parameters are derived from the luminosity-weighted fitting in inner region of $S/N > 10$ (corresponding to about 23 V -magnitude) in this paper, while the ratio in RC3 is measured at the contour of 25 B -magnitude. That is, our results are obtained from inner disk, in which the bar or spiral arms sometimes dominate, while the PA in RC3 is measured at outer disk. These structure are apparent in face-on galaxies and often cause the discrepancy of the PAs.

We compare the model disk axial ratio $(b/a)_d$ obtained in surface brightness fitting with the catalogue axial ratios R_{25} taken from RC3. The comparison is shown in figure 9. The model axial ratio is generally consistent with R_{25} in RC3.

The bulge axial ratio $(b/a)_b$ for some galaxies are larger than 1.0 in table 3-5. That is, the major- and minor-axis for these bulge is reverse against the disk. In other words, the $(b/a)_b > 1$ indicates that the PA of bulge is nearly vertical to that of disk. The $(b/a)_b > 1$ would be due to a distorted structure of bulge. If we construct the model including parameters of individual PAs for both bulge and disk, the $(b/a)_b > 1$ would not happen. To simplify, we do not use the parameters of individual PAs for bulge and disk in model, however. When $(b/a)_b$ is larger than 1, the intrinsic eccentricity $\epsilon = \sqrt{1 - (b/a)_b^2}$ cannot be calculated and therefore the $(M/L)_b$ also cannot be obtained. We apply $\epsilon = 0.0$ (assuming spherical bulge) to calculate the M/L_b if the ϵ cannot be calculated. Fortunately, the dependence of $(M/L)_b$ on ϵ is relatively small; smaller than 10% within $0 \leq \epsilon < 1$. Therefore the error is not so large even if we assume the spherical bulge, and therefore the uncertainty of bulge PA does not considerably affect the resulting M/L .

4.4. Dust Extinction

The bulge and disk colors are listed in table 6. Figure 10 shows the color-color ($V - I$ versus $I - J$) diagram. The mesh in the figure represents W94 model of single starburst with Salpeter IMF, the age = 1.5 to 17 Gyr, and $[\text{Fe}/\text{H}] = -2.0$ to 0.5. We find that our data points

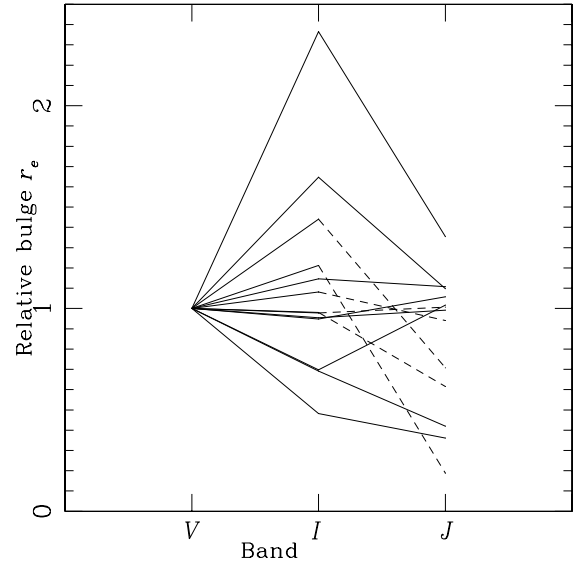


Fig. 7. The trend of bulge effective radius r_e on bands for 13 galaxies. The r_e is normalized to that of V band. The dashed lines are unreliable data (NGC 2903, 3198, 4258, 4321 and 4535 in the J band).

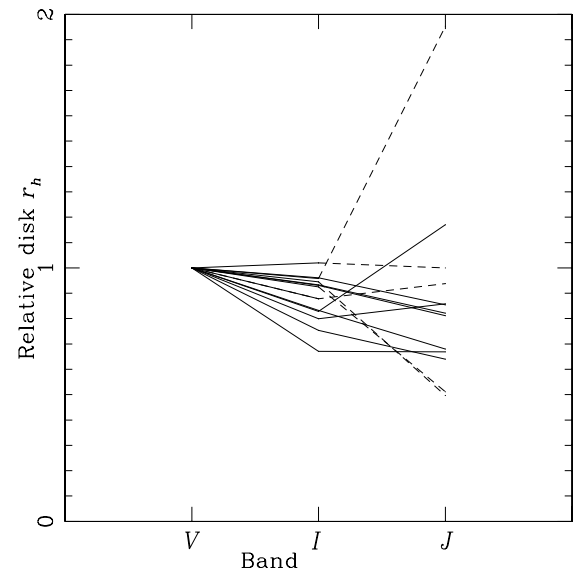


Fig. 8. The trend of disk scale length r_h on bands for 13 galaxies. The r_h is normalized to that of V band. The dashed lines are unreliable data (NGC 2903, 3198, 4258, 4321 and 4535 in the J band).

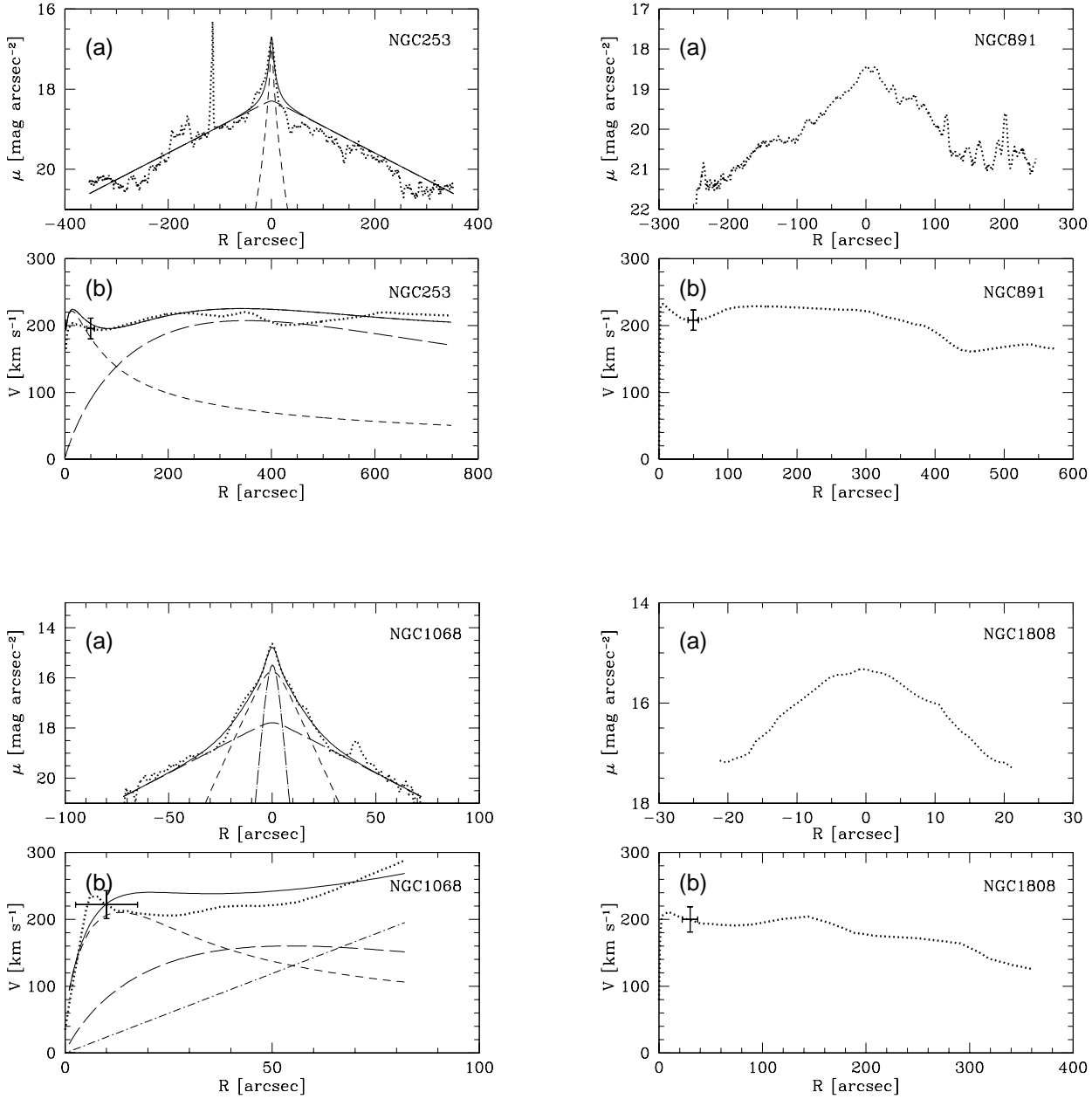
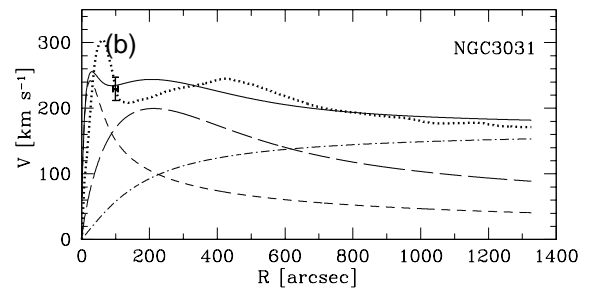
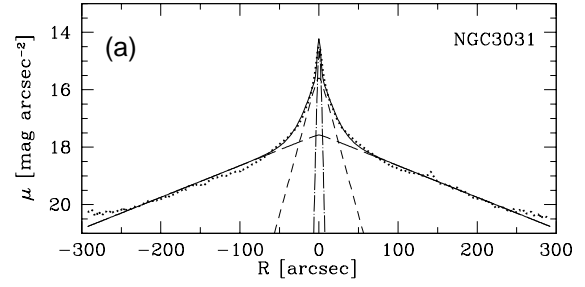
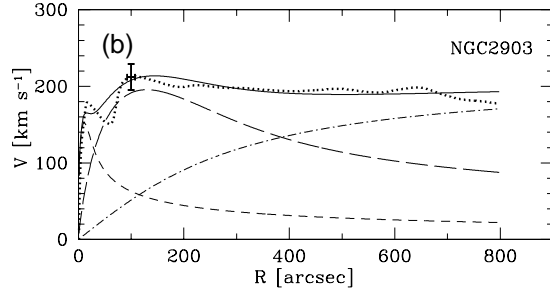
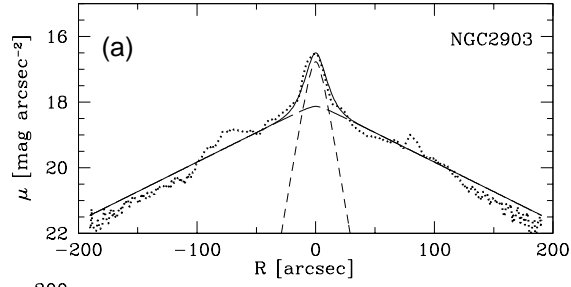
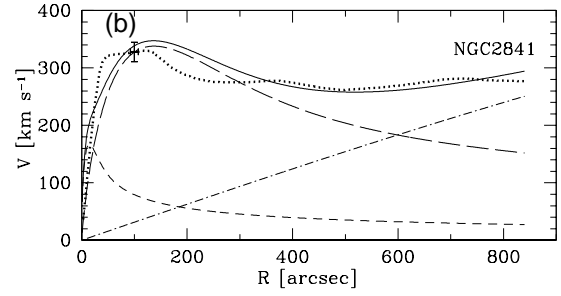
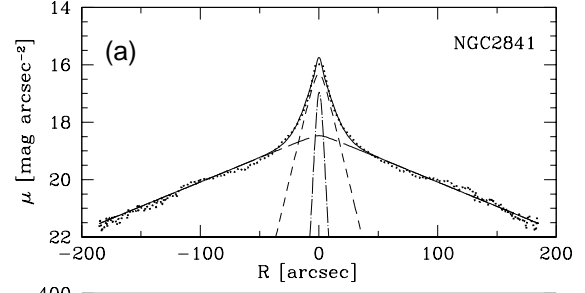
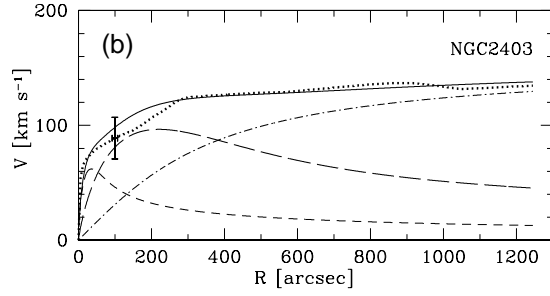
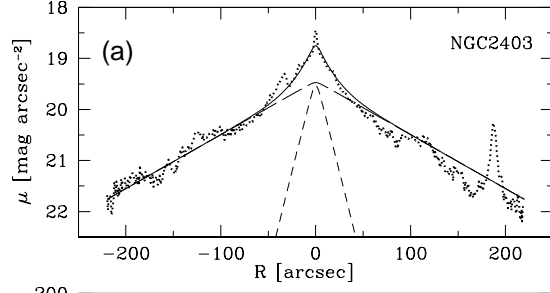
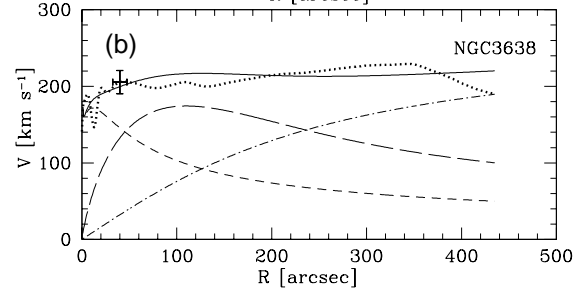
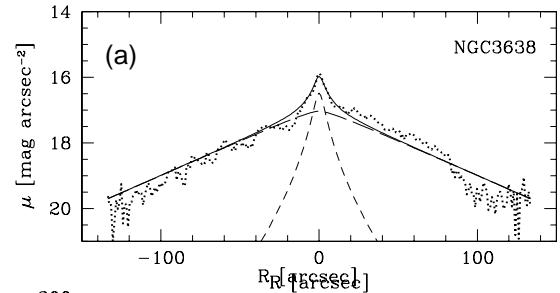
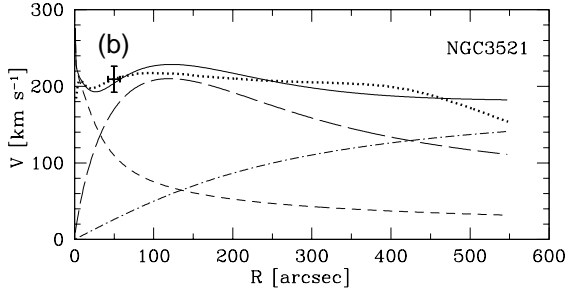
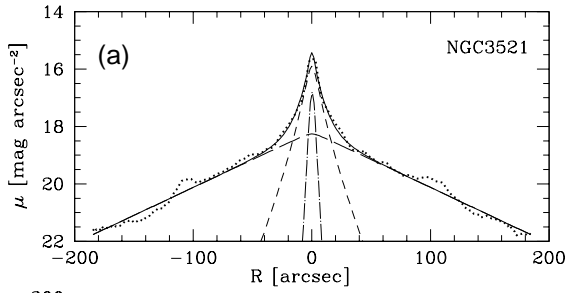
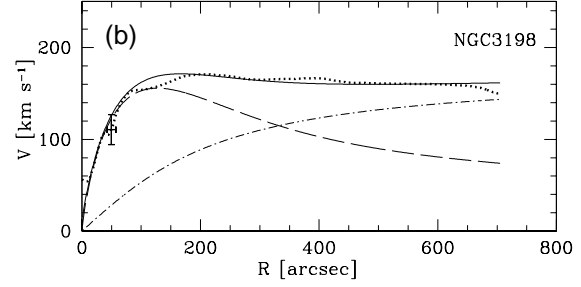
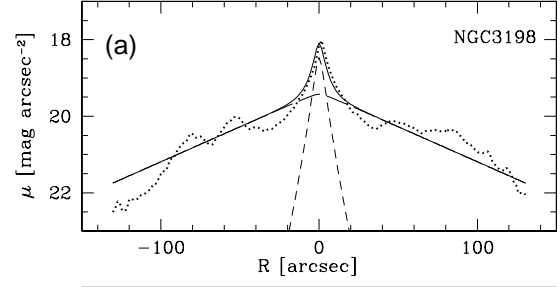
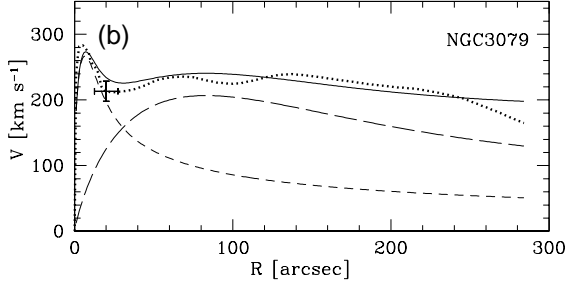
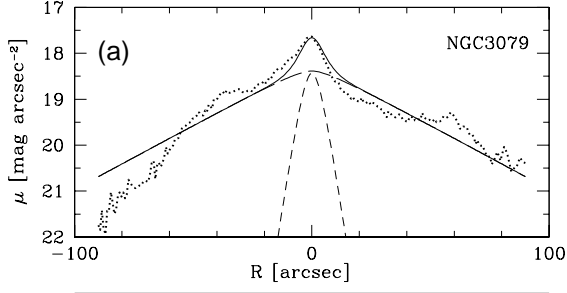
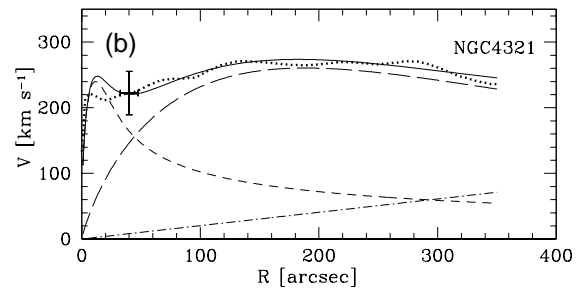
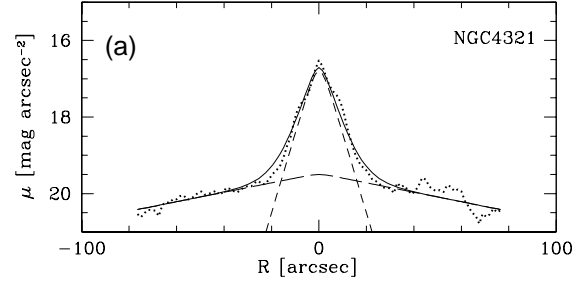
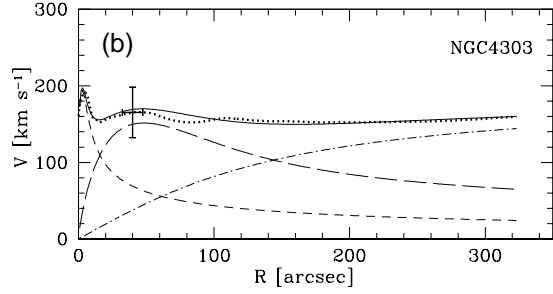
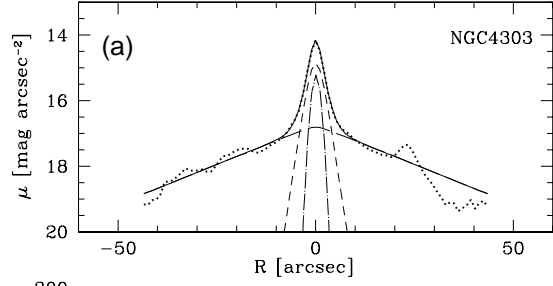
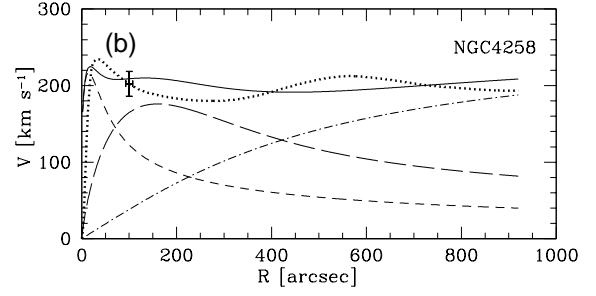
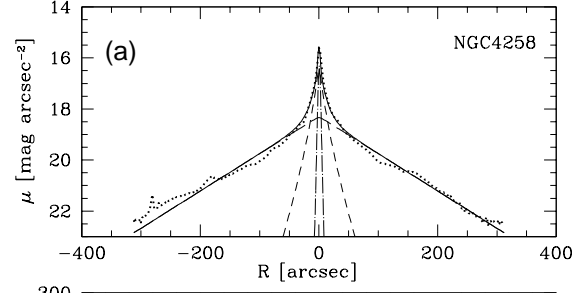
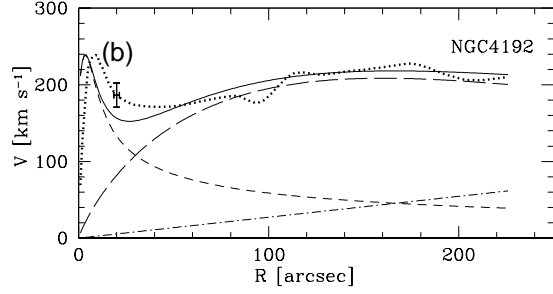
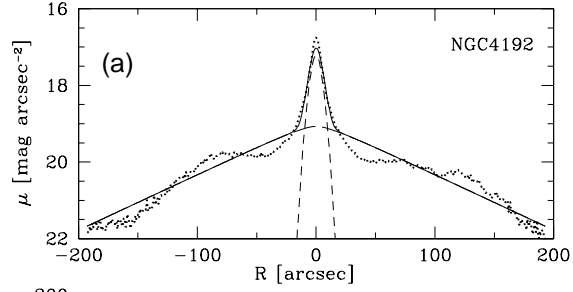
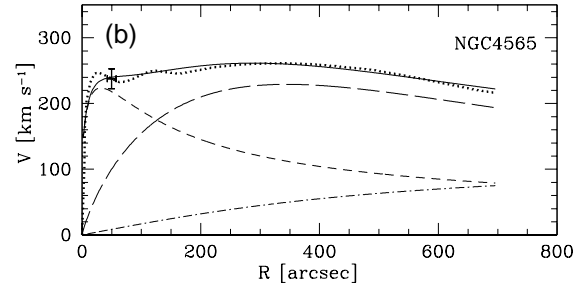
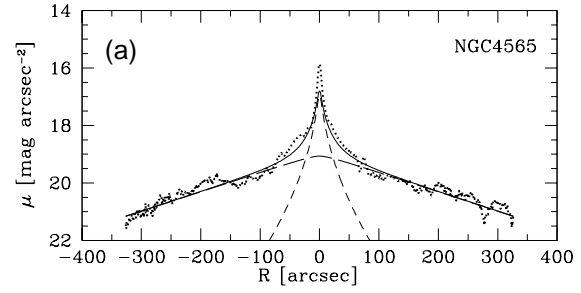
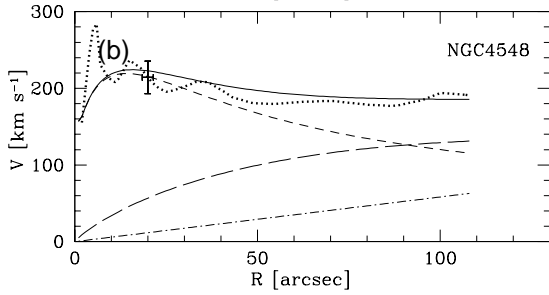
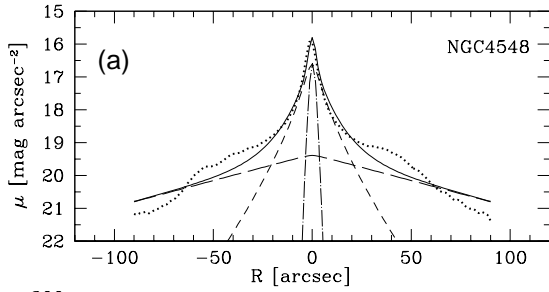
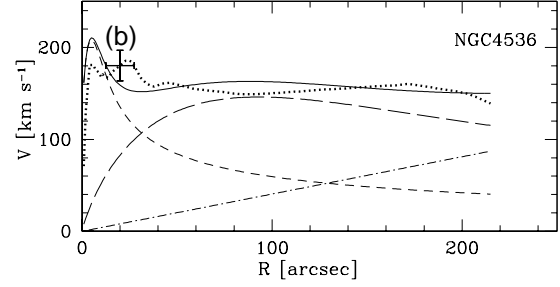
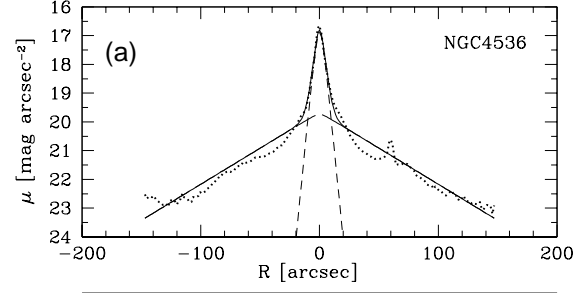
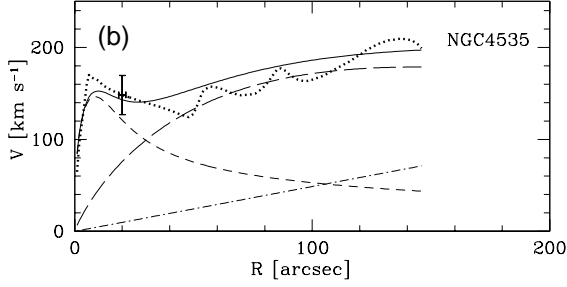
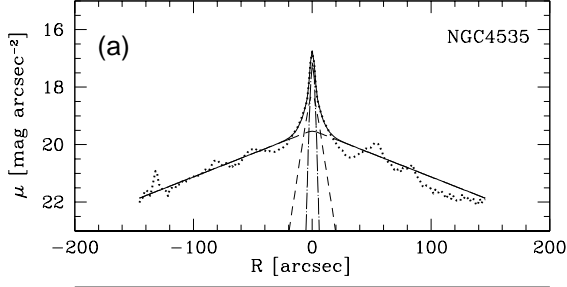


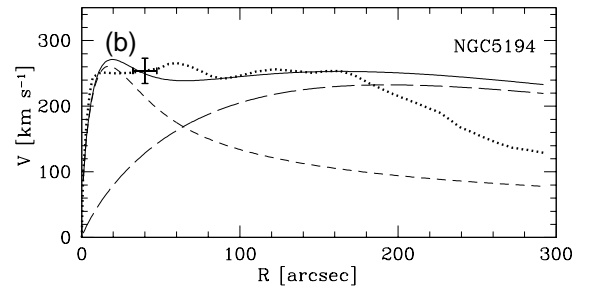
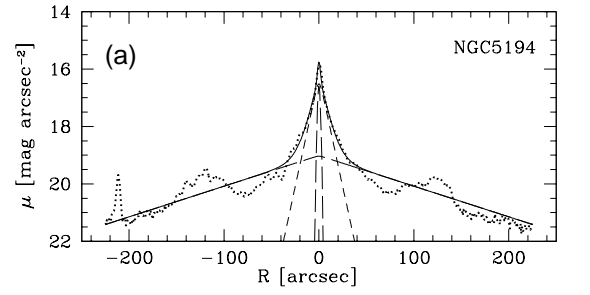
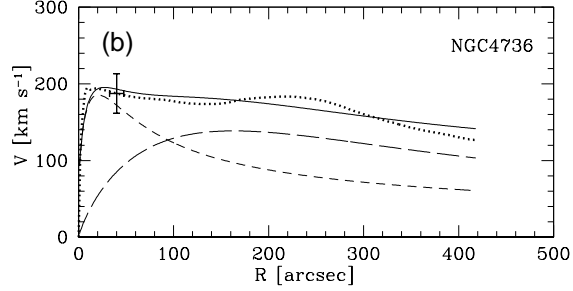
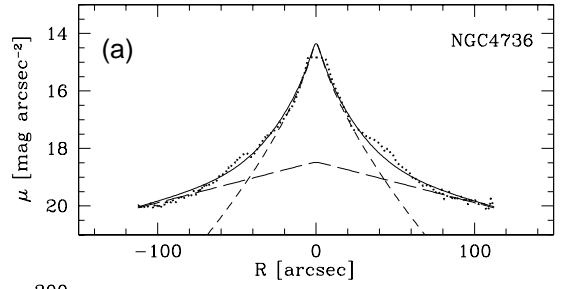
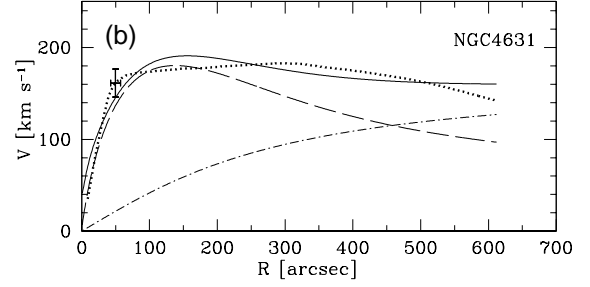
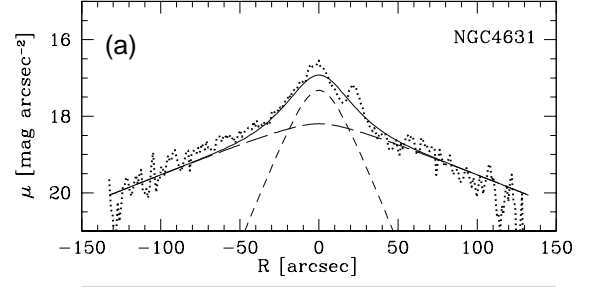
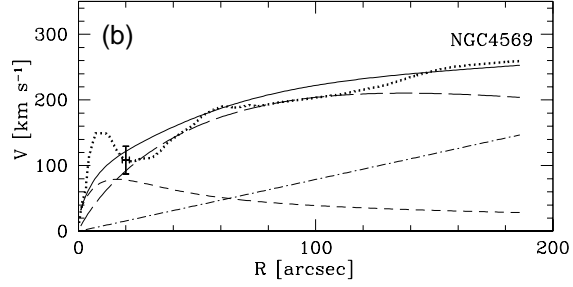
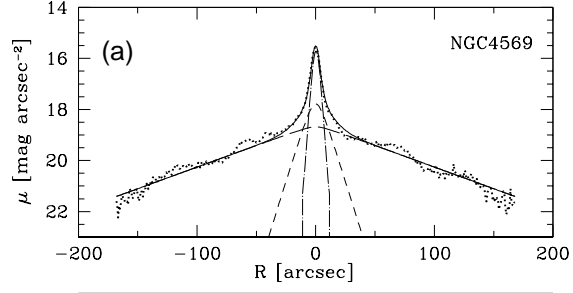
Fig. 6. (a) observed and model surface brightness profiles along major axis. The dotted lines, solid lines, short-dashed lines, long-dashed lines and dot-long dashed lines represent the observed profile, the model profile, bulge, disk and nuclear contributions, respectively. The profiles of NGC 1808, NGC 3628, NGC 4303 and NGC 4631 are those of *J* band images, and the remainder are those of *I* band images. (b) observed and model rotation curves. The symbols are the same as for (a). The contribution from dark halo is shown as the dot-dashed lines. The error bars for the rotation curves represent the angular resolution of 15 arcsec (Sofue 1997) or 3 arcsec (Sofue et al. 2003), and the velocity resolution of 15 km s⁻¹/sin(*i*) for both of Sofue (1997) and Sofue et al. (2003), where *i* is the inclination of galaxy.











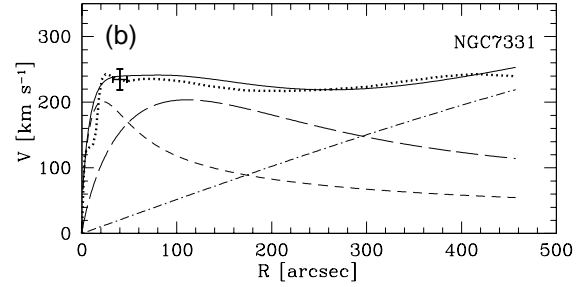
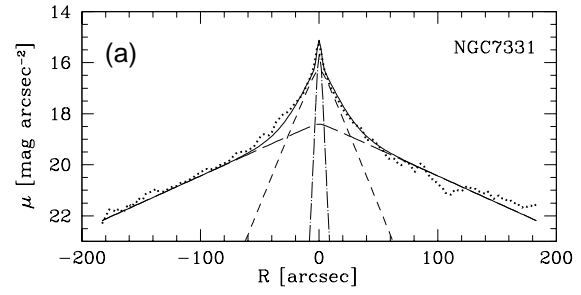
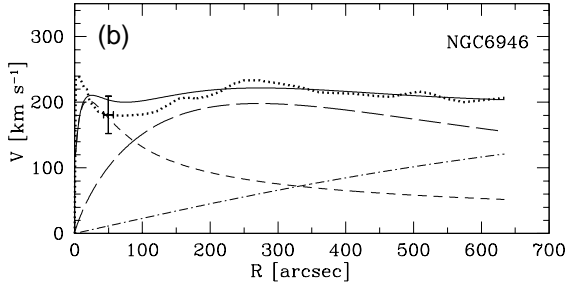
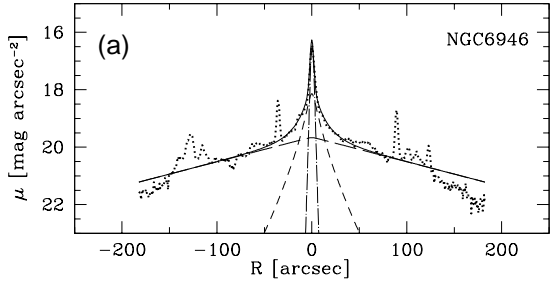
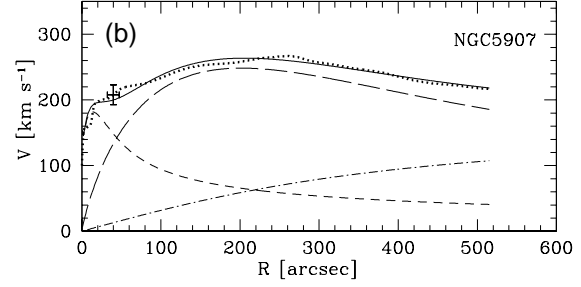
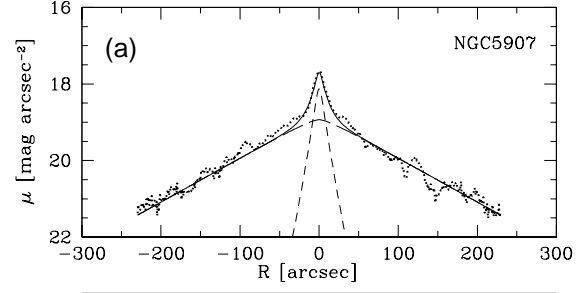
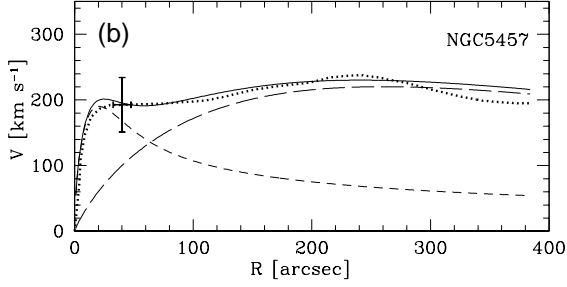
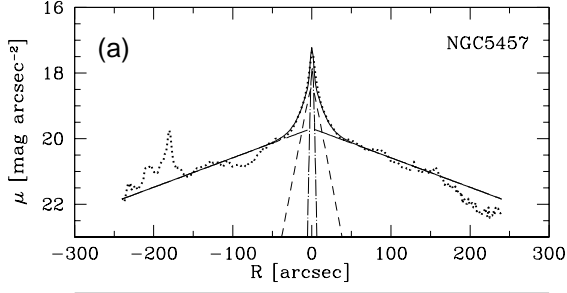


Table 3. Results of V band surface brightness fitting.

Name (1)	μ_e (2)	$(b/a)_b$ (3)	r_e (4)	β (5)	μ_0 (6)	$(b/a)_d$ (7)	r_h (8)	L_B (9)	L_D (10)	L_T (11)	B/T (12)	nuclear (13)	error (14)
N 253	21.63	1.51	11.60	1/2	19.80	0.27	196.20	12.82	7.92	7.91	0.01	-	0.25
N 891	-	-	-	-	-	-	-	-	-	-	-	-	no fit
N 1068	17.96	0.63	9.98	1	18.83	0.91	30.90	10.78	9.48	9.10	0.21	11.83	0.15
N 2403	22.11	1.29	20.99	1	20.15	0.60	108.63	12.53	8.54	8.52	0.03	-	0.41
N 2841	18.79	0.69	10.96	1	19.64	0.41	68.41	11.29	9.43	9.23	0.15	13.33	0.25
N 2903	18.94	0.54	8.41	1	19.12	0.48	62.91	12.29	8.93	8.88	0.04	-	0.19
N 3031	18.46	0.74	25.76	1	19.07	0.61	147.00	9.04	6.85	6.71	0.12	12.94	0.15
N 3079	21.30	0.46	10.90	1	19.60	0.23	46.76	14.27	10.86	10.82	0.04	-	0.24
N 3198	21.43	0.87	5.75	3/4	20.41	0.38	64.08	14.95	10.44	10.43	0.02	-	0.18
N 3521	18.36	0.53	9.27	2/3	19.21	0.53	58.03	11.32	9.09	8.95	0.11	15.16	0.26
N 4192	17.91	0.75	3.02	1	19.99	0.23	82.57	13.12	10.02	9.96	0.06	-	0.20
N 4258	18.57	0.30	10.34	2/3	19.54	0.51	78.55	11.89	8.80	8.74	0.06	16.01	0.26
N 4321	19.12	0.81	7.96	1	20.49	0.70	85.91	12.15	9.21	9.14	0.06	-	0.19
N 4535	20.96	0.73	6.84	1	20.80	0.80	76.13	14.43	9.65	9.63	0.01	16.24	0.25
N 4536	19.46	0.72	4.10	1	21.09	0.67	52.52	14.06	10.94	10.88	0.05	-	0.27
N 4548	20.42	0.87	14.13	2/3	20.93	0.55	85.29	11.93	9.94	9.78	0.14	15.88	0.12
N 4565	22.18	0.94	55.23	1/2	20.50	0.07	199.38	10.52	10.11	9.54	0.41	-	0.37
N 4569	19.90	0.73	9.30	1	19.86	0.39	72.13	12.70	9.58	9.43	0.05	12.12	0.13
N 5194	19.13	1.21	11.98	1	20.01	0.73	112.25	10.84	8.13	8.04	0.08	13.98	0.27
N 5457	21.14	1.26	15.26	1	20.80	0.98	149.69	12.27	8.07	8.05	0.02	16.20	0.22
N 5907	21.41	0.29	21.23	3/4	20.46	0.10	124.91	13.27	10.56	10.48	0.08	-	0.18
N 6946	20.23	1.21	8.06	2/3	19.93	0.82	135.73	12.59	7.55	7.54	0.01	14.42	0.39
N 7331	18.66	0.38	16.65	1	19.68	0.42	64.47	10.90	9.57	9.29	0.23	14.55	0.26

The colons denote unreliable data (see text).

(1) NGC Number. (2) Bulge effective luminosity [mag arcsec⁻²]. (3) Bulge axial ratio. (4) Bulge effective radius [arcsec]. (5) Bulge shape index $\beta = 1/n$. (6) Disk central luminosity [mag arcsec⁻²]. (7) Disk axial ratio. (8) Disk scale length [arcsec]. (9) Total luminosity of bulge [mag]. (10) Total luminosity of disk [mag]. (11) Total luminosity of the galaxy [mag]. (12) Bulge-to-total (bulge plus disk) luminosity ratio. (13) Nucleus (central point source) luminosity [mag]. (14) Total residual in magnitude unit.

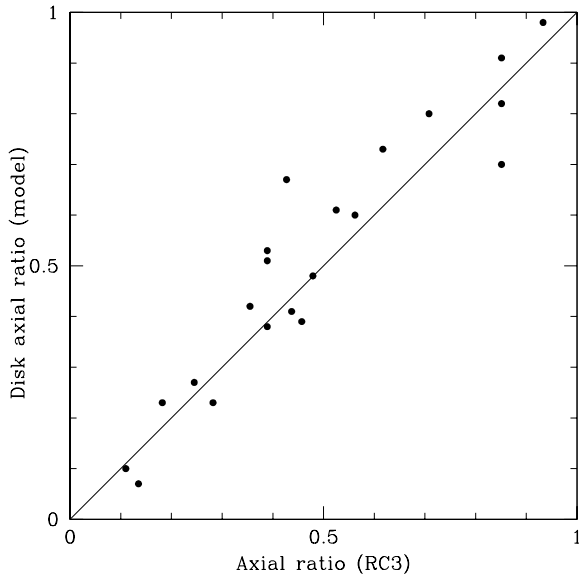


Fig. 9. The comparison of the disk axial ratio $(b/a)_d$ obtained from the fitting in the present study with the catalogue axial ratios taken from RC3. The model $(b/a)_d$ is for V band, while that of RC3 is derived from the contour of 25 B magnitude. The solid line shows the equality.

somewhat deviate from W94 model. That is, our data are somewhat bluer in $V-I$ than W94 model as a whole. The discrepancy would be ascribed to the assumption of W94 model considering only a single stellar population of old age (> 1.5 Gyr) and of low mass stars ($< 2.0 M_\odot$). If young massive stars exist in the galaxy, the $V-I$ would be bluer than the W94 model but the $I-J$ would not be considerably influenced, because the young massive stars radiate mainly in bluer bands. We find that the data points do not considerably shift into the direction of the absorption vector. The exception is the bulge of dusty galaxy NGC 253 ($V-I = 2.60$, $I-J = 1.69$), which locates in the direction of the absorption vector (out of the diagram). In addition, the color of NGC 3079 bulge is abnormal: $V-I = 1.01$ and $I-J = 2.56$. Both NGC 253 and NGC 3079 are high-inclination (nearly edge-on) and the bulge parameters would be seriously influenced by dust extinction. The bulge of NGC 6946 ($V-I = 1.96$, $I-J = 0.93$) would be also reddened by dust. Comparing our result with W94 models, we note that the most galaxies of low-inclination except for NGC 6946 would not be seriously affected by internal dust extinction.

Figure 11 shows the diagram of $V-I$ color versus inclination i , which is quoted from RC3. In general, since the internal extinction is higher in the galactic center, the bulge luminosity would be affected more strongly by

Table 4. Results of I band surface brightness fitting.

Name (1)	μ_e (2)	$(b/a)_b$ (3)	r_e (4)	β (5)	μ_0 (6)	$(b/a)_d$ (7)	r_h (8)	L_B (9)	L_D (10)	L_T (11)	B/T (12)	nuclear (13)	error (14)
N 253	19.86	1.20	19.12	1/2	18.23	0.28	163.32	10.22	6.65	6.61	0.04	-	0.22
N 891	-	-	-	-	-	-	-	-	-	-	-	-	no fit
N 1068	16.79	0.59	9.77	1	17.59	0.92	25.29	9.72	8.67	8.23	0.25	11.04	0.13
N 2403	21.10	1.14	24.33	1	19.36	0.60	102.73	11.34	7.87	7.83	0.04	-	0.38
N 2841	17.52	0.72	10.46	1	18.35	0.42	63.81	10.09	8.26	8.06	0.15	12.64	0.19
N 2903	17.42	0.42	8.24	1	17.97	0.46	60.26	11.09	7.92	7.86	0.05	-	0.15
N 3031	16.99	0.76	17.99	1	17.39	0.62	98.66	8.32	5.95	5.83	0.10	12.18	0.10
N 3079	19.06	0.63	5.25	1	18.12	0.24	38.70	13.26	9.73	9.69	0.04	-	0.18
N 3198	20.17	0.90	6.97	3/4	19.33	0.37	59.28	13.24	9.56	9.52	0.03	-	0.15
N 3521	17.45	0.57	10.63	2/3	18.06	0.58	55.78	10.04	7.93	7.79	0.13	13.96	0.18
N 4192	16.55	0.62	3.36	1	18.80	0.23	74.53	11.73	9.03	8.94	0.08	-	0.18
N 4258	18.48	0.53	14.89	2/3	18.26	0.55	74.24	10.41	7.56	7.49	0.07	14.04	0.22
N 4321	18.09	0.73	8.61	1	19.42	0.75	87.64	11.06	8.03	7.97	0.06	-	0.08
N 4535	19.52	0.85	6.69	1	19.46	0.80	66.81	12.87	8.59	8.56	0.02	15.12	0.22
N 4536	17.62	0.64	4.22	1	19.62	0.66	43.20	12.29	9.90	9.79	0.10	-	0.26
N 4548	18.75	0.83	14.08	2/3	19.28	0.74	67.48	10.31	8.46	8.28	0.15	14.50	0.14
N 4565	19.98	0.79	37.57	1/2	18.91	0.08	160.37	9.33	8.78	8.27	0.38	-	0.33
N 4569	18.80	0.59	12.05	1	18.47	0.38	63.90	11.27	8.51	8.31	0.07	10.79	0.13
N 4736	16.70	0.99	17.66	2/3	18.42	0.70	75.92	7.58	7.42	6.75	0.46	-	0.11
N 5194	18.03	1.24	11.86	1	18.94	0.75	101.70	9.73	7.24	7.13	0.09	13.27	0.26
N 5457	20.00	1.31	14.42	1	19.67	1.00	120.95	11.22	7.33	7.30	0.03	15.49	0.18
N 5907	19.75	0.36	14.66	3/4	18.75	0.10	94.23	12.19	9.40	9.32	0.07	-	0.19
N 6946	19.71	0.82	19.07	2/3	18.98	0.82	126.33	10.63	6.75	6.72	0.03	12.29	0.28
N 7331	17.48	0.41	15.78	1	18.15	0.46	51.51	9.77	8.44	8.15	0.22	13.28	0.21

The colons denote unreliable data (see text).

(1) NGC Number. (2) Bulge effective luminosity [mag arcsec⁻²]. (3) Bulge axial ratio. (4) Bulge effective radius [arcsec]. (5) Bulge shape index $\beta = 1/n$. (6) Disk central luminosity [mag arcsec⁻²]. (7) Disk axial ratio. (8) Disk scale length [arcsec]. (9) Total luminosity of bulge [mag]. (10) Total luminosity of disk [mag]. (11) Total luminosity of the galaxy [mag]. (12) Bulge-to-total (bulge plus disk) luminosity ratio. (13) Nucleus (central point source) luminosity [mag]. (14) Total residual in magnitude unit.

the extinction than the disk luminosity (e.g., Peletier et al. 1999). We find that the bulges are generally somewhat redder than the disks.

Figure 12 shows the diagram of M/L_V (M/L of V band), which would be sensitive to the dust extinction, versus inclination i . The bulge M/L_V for some galaxies are significantly higher than normal values predicted with various stellar population synthesis models: about 1 to 10. The high values (about 20 to 100) would be caused by two reasons; One is the dust extinction, and the other is the error of model fitting for rotation curve. The former reason would be valid for bulges of nearly edge-on ($i > 75^\circ$) galaxies (NGC 253, NGC 3079, NGC 4565 and NGC 5907), however the color is not significantly red except for NGC 253. The latter reason would be suitable for most of those data, because the bulge effective magnitude $\mu_{e,V}$ is significantly large (NGC 253, 2403, 3079, 3198, 4535, 4565, 5457, 5907 and 6946) and thus unreliable as mentioned in section 3.4. Takamiya, Sofue (2000) has claimed that the high bulge M/L for low luminosity galaxies may be caused by the dark matter concentration in the core region other than old stars or dust extinction. To focus on stellar population, however, we use only reliable data. We consider that the bulge M/L or bulge $V-I$ outside the reliable range of bulge μ_e , disk μ_0 or

with $i > 75^\circ$ would be influenced by error of fitting or dust extinction, and thus are excluded from the following discussion.

For the reliable sample, the average values of bulge M/Ls for V , I , J bands are 4.5 ± 2.3 (13 sample), 2.7 ± 1.7 (14 sample) and 1.0 ± 0.2 (5 sample), respectively. They do not include the nearly edge-on ($i > 75^\circ$) galaxies. The disk M/Ls for V , I , J bands are 2.0 ± 0.7 (17 sample), 1.4 ± 0.5 (21 sample) and 0.7 ± 0.3 (11 sample), respectively. The average of bulge $V-I$ is 1.33 ± 0.30 (18 sample) and that of disk $V-I$ is 1.05 ± 0.20 (22 sample).

5. Discussion

5.1. The Comparison with Galaxy Evolution Models

We compare the obtained colors and M/Ls with galaxy evolution models in figures 13-15. Only reliable data as mentioned in the previous section are plotted. The mesh in the figure represents W94 model of single starburst formation with Salpeter IMF, the age = 1.5 to 17 Gyr, and $[\text{Fe}/\text{H}] = -2.0$ to 0.5. When we compare the obtained colors and M/Ls with those of W94 model, we estimate the luminosity-weighted average age and metallicity of the system represented by the single star formation. The two lines represent the model sequences taken from

Table 5. Results of J band surface brightness fitting.

Name (1)	μ_e (2)	$(b/a)_b$ (3)	r_e (4)	β (5)	μ_0 (6)	$(b/a)_d$ (7)	r_h (8)	L_B (9)	L_D (10)	L_T (11)	B/T (12)	nuclear (13)	error (14)
N253	16.50	0.57	12.74	1/2	16.39	0.45	133.50	8.53	4.67	4.64	0.03	-	0.11
N 891	-	-	-	-	-	-	-	-	-	-	-	-	no fit
N2841	16.61	0.40	10.87	1	16.92	0.52	56.15	9.71	6.88	6.76	0.07	10.32	0.13
N2903	14.94:	0.38:	5.18:	1:	17.17:	0.28:	122.86:	9.70:	6.13:	6.09:	0.04:	-	0.10
N3031	15.86	0.65	26.19	1	16.29	0.57	98.34	6.54	4.95	4.70	0.18	8.84	0.11
N3079	15.80	0.59	3.93	1	16.98	0.13	54.70	10.70	8.48	8.35	0.11	-	0.14
N3198	17.76:	0.82:	1.08:	3/4:	17.68:	0.36:	32.72:	14.54:	9.23:	9.22:	0.01:	-	0.17
N3521	16.17	0.74	10.27	2/3	16.45	0.53	49.58	8.55	6.67	6.49	0.15	-	0.09
N3628	19.09	0.86	16.87	1/2	16.84	0.20	51.14	10.08	8.05	7.89	0.13	-	0.16
N4258	16.43:	0.61:	7.31:	2/3:	16.37:	0.54:	38.95:	9.75:	7.10:	7.00:	0.08:	12.76:	0.15
N4303	15.73	0.99	2.27	1	16.71	0.75	22.38	11.26	8.28	8.20	0.06	13.11	0.18
N4321	16.72:	0.69:	7.49:	1:	18.25:	0.67:	85.94:	10.06:	7.03:	6.96:	0.06:	-	0.14
N4535	18.58:	0.69:	6.89:	1:	18.77:	0.91:	71.38:	12.10:	7.61:	7.59:	0.02:	12.98:	0.13
N4536	-	-	-	-	-	-	-	-	-	-	-	-	no fit
N4631	17.08	0.15	16.71	1	17.75	0.19	64.16	10.31	8.55	8.35	0.17	-	0.27
N4736	13.49:	1.08:	2.29:	2/3:	15.28:	0.76:	23.35:	8.63:	6.74:	6.56:	0.15:	-	0.24
N5907	17.90	0.49	8.91	3/4	16.89	0.09	79.96	11.09	8.01	7.95	0.06	-	0.12
N6946	17.62	0.86	10.92	2/3	17.85	0.75	110.02	9.70	5.99	5.95	0.03	11.92	0.37
N7331	16.20	0.38	17.62	1	16.87	0.47	55.31	8.32	6.98	6.69	0.22	11.15	0.28

The colons denote unreliable data (see text).

(1) NGC Number. (2) Bulge effective luminosity [mag arcsec⁻²]. (3) Bulge axial ratio. (4) Bulge effective radius [arcsec]. (5) Bulge shape index $\beta = 1/n$. (6) Disk central luminosity [mag arcsec⁻²]. (7) Disk axial ratio. (8) Disk scale length [arcsec]. (9) Total luminosity of bulge [mag]. (10) Total luminosity of disk [mag]. (11) Total luminosity of the galaxy [mag]. (12) Bulge-to-total (bulge plus disk) luminosity ratio. (13) Nucleus (central point source) luminosity [mag]. (14) Total residual in magnitude unit.

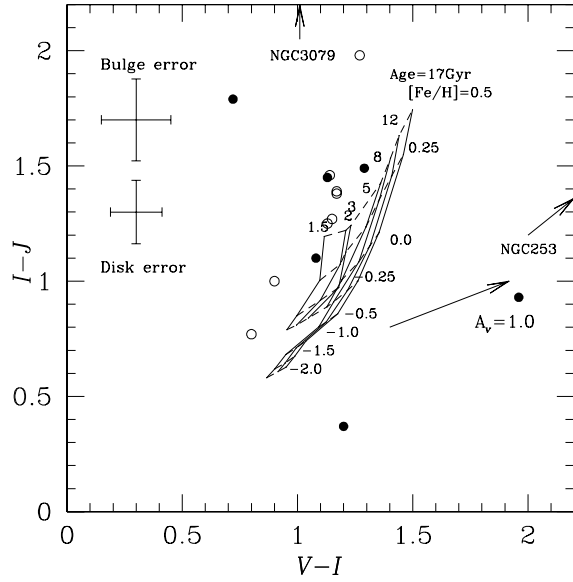


Fig. 10. Color-color diagram for the bulge (filled circles) and disks (open circles). The error bars represent the typical errors for bulge and disk. The models of Worthey (1994) of the same age are connected by solid lines, while the models of the same metallicity are connected by dashed lines. The bulges of NGC 253 and NGC 3079 are outside the figure and locate in the directions of the arrows.

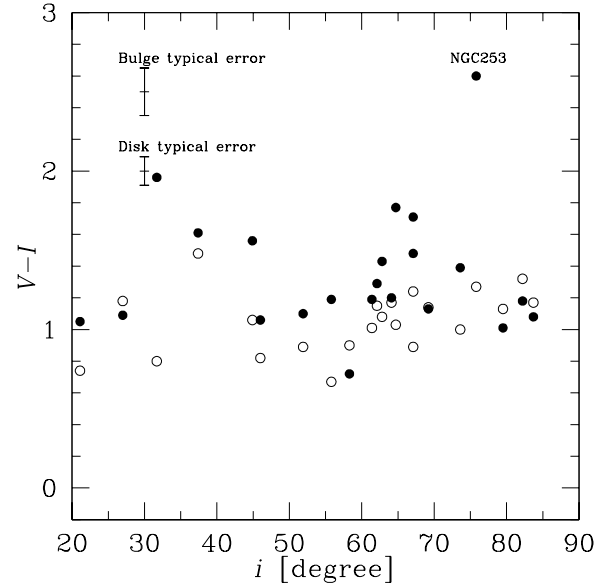


Fig. 11. The inclination i versus $V-I$ diagram. The filled and open circles represent bulge and disk, respectively.

Table 6. Colors of bulges and disks.

Name	$(V-I)_b$	$(V-I)_d$	$(I-J)_b$	$(I-J)_d$
(1)	(2)	(3)	(4)	(5)
N 253	2.60	1.27	1.69	1.98
N 891	-	-	-	-
N 1068	1.06	0.82	-	-
N 2403	1.19	0.67	-	-
N 2841	1.20	1.17	0.37	1.38
N 2903	1.19	1.01	1.39:	1.79:
N 3031	0.72	0.90	1.79	1.00
N 3079	1.01	1.13	2.56	1.25
N 3198	1.71	0.89	-1.31:	0.33:
N 3521	1.29	1.15	1.49	1.27
N 4192	1.39	1.00	-	-
N 4258	1.48	1.24	0.66:	0.46:
N 4321	1.09	1.18	1.01:	1.00:
N 4535	1.56	1.06	0.77:	0.97:
N 4536	1.77	1.03	-	-
N 4548	1.61	1.48	-	-
N 4565	1.18	1.32	-	-
N 4569	1.43	1.08	-	-
N 4736	-	-	-1.04:	0.68:
N 5194	1.10	0.89	-	-
N 5457	1.05	0.74	-	-
N 5907	1.08	1.17	1.10	1.39
N 6946	1.96	0.80	0.93	0.77
N 7331	1.13	1.14	1.45	1.46

The colons denote unreliable data (see text).

(1) NGC Number. (2) Bulge $V-I$. (3) Disk $V-I$. (4) Bulge $I-J$. (5) Disk $I-J$.

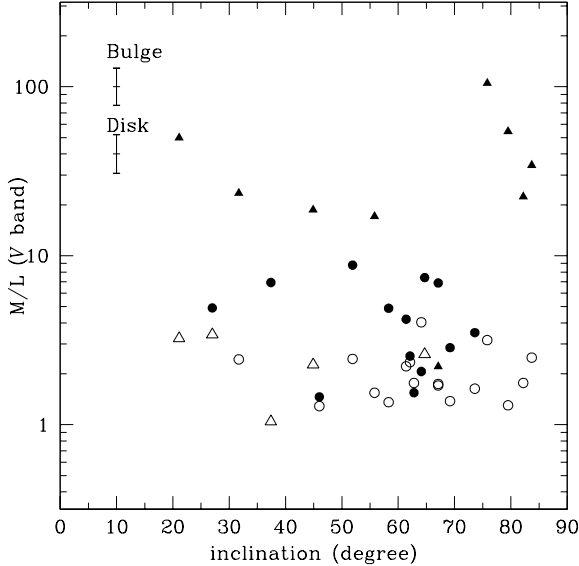


Fig. 12. The inclination i versus M/L_V diagram. The filled and open circles represent bulge and disk in the reliable range of rotation curve fitting ($\mu_{e,V} < 20.5$, $\mu_{0,V} < 20.5$), respectively. The filled and open triangles represent unreliable data of bulge and disk, respectively.

BD01, which are based on an exponentially declining SFR model of GISSEL96 (see Bruzual, Charlot 1993; Leitherer et al. 1996) with various time-scale τ and IMFs. Here we show the two models with IMFs of Salpeter (1955) and Scalo (1986) in the figures. The formation epoch and the metallicity are 12 Gyr and $Z=0.02$, respectively, and τ varies from 1 to infinity for both of two models. The upper-right parts of the lines correspond to the models of small τ , which consist of only old population, whereas the lower-left parts of the lines correspond to the models of large τ , which include relatively young population. The color and M/L inferred from small τ models are consistent with those from W94 model at 12 Gyr with $[\text{Fe}/\text{H}]=0.0$.

In general, the M/L is significantly sensitive to massive young stars in the system. BD01 has claimed that a large secondary starburst (10 % mass of the galaxy changes into stars) decreases the system M/L at a given color by up to a factor of 3. In addition, the difference of IMF also considerably affects the zero-point of the color- M/L correlation, especially in near-infrared band, while the choice of stellar population synthesis model does not notably change the zero-point. The sensitivity of the zero-point of the color- M/L correlation to the IMF is due entirely to differences in the number of low-mass stars in each IMF (BD01). Since Scalo IMF produces less low-mass stars than Salpeter IMF, the model with Scalo IMF yields lower M/L at a given color than the model with Salpeter IMF.

Table 7. V band M/L ratios and halo parameters.

Name	$(M/L_V)_b$	$\sigma_{(M/L_V)_b}$	$(M/L_V)_d$	$\sigma_{(M/L_V)_d}$	σ_h	R_h	rms
(1)	(2)	(3)	(4)	(5)	(6)	(7)	(8)
N 253	104.94:	85.88	3.17	0.59	-	-	26.07
N 891	-	-	-	-	-	-	no fit
N 1068	1.46	0.46	1.29	0.43	-	-	25.66
N 2403	17.10:	7.93	1.54	0.73	110.74	0.31	3.03
N 2841	2.06	0.40	4.04	0.61	-	-	47.91
N 2903	4.21	1.26	2.22	0.48	157.45	0.27	11.77
N 3031	4.89	1.02	1.36	0.44	100.44	0.20	21.71
N 3079	54.28:	24.20	1.30	0.33	114.16	0.09	35.63
N 3198	2.21:	1.64	1.71	0.57	125.95	0.21	5.19
N 3521	2.55	0.54	2.34	0.66	138.95	0.25	14.72
N 4192	3.51	0.64	1.63	0.31	-	-	33.38
N 4258	6.89	1.27	1.74	0.50	202.97	0.51	31.09
N 4321	4.91	1.63	3.41	1.29	-	-	4.11
N 4535	18.70:	9.93	2.26:	0.71	-	-	12.24
N 4536	7.42	1.89	2.61:	1.21	-	-	20.46
N 4548	6.94	2.48	1.04:	0.52	-	-	13.56
N 4565	22.33:	8.54	1.77:	0.63	-	-	17.82
N 4569	1.55	0.94	1.76	0.40	-	-	24.83
N 5194	8.79	2.33	2.45	0.57	-	-	46.43
N 5457	49.88:	19.06	3.24:	2.07	-	-	3.67
N 5907	34.32:	13.39	2.49	0.47	-	-	19.66
N 6946	23.46:	12.25	2.43	1.02	-	-	3.70
N 7331	2.86	0.64	1.38	0.41	-	-	16.58

The colons denote unreliable data (see text).

(1) NGC Number. (2) Bulge M/L at the V band. (3) 1σ error of the bulge M/L . (4) Disk M/L at the V band.

(5) 1σ error of the disk M/L . (6) Halo velocity dispersion in $10^2[\text{km s}^{-1}]$ unit. (7) Halo core radius [kpc].

(8) Residual in $[\text{km s}^{-1}]$ unit.

It is known that continuous star forming models also give the similar result as the model of shallower slope IMF + exponentially declining SFR, however BD01 have not give the values of M/L s and colors using continuous star forming models. Note that continuous star formation models may be suitable as well as the models of shallower slope IMF + exponentially declining SFR.

We find in the (a) part of figures 13-15 that the color and M/L s for both bulges and disks are generally in good agreement with the models. In general bulges have higher M/L s and redder color than disks in the figures. The (b) part of figures 13-15 show the comparison of the bulge with the counterpart disk for the same galaxy in the M/L -color diagrams. We find that the bulges have generally higher M/L and redder color than the counterpart disk in the galaxy. Although the trend would be partially caused by the dust extinction, the direction of the connected lines of the galaxies are somewhat different from the extinction vector in many cases. We therefore conclude that bulges are generally older than disks. However, some bulges have almost the same or lower M/L s and colors as disks. These bulges should be as young as disks.

The effects of age, metallicity, IMF and dust extinction almost degenerate in the V band (figure 13). On the other hand, the degeneracy of age, metallicity and dust extinction is resolved in the I band (figure 14), and the difference of IMF is resolved in the J band (figure 15), in

which the effect of dust extinction is smaller than in the V band. Most of bulges and disks agree with the model with the exponentially declining SFR. In addition, the Scalo or shallower slope IMF is appropriate in the J band (figure 15), though the data points are scarce. The M/L values of W94 model at the J band are somewhat different from our results. The discrepancy would be due to the IMF used in W94; the Salpeter IMF tends to produce higher M/L than Scalo or other shallower slope IMFs at the J band rather than at the V and I band. The figures 13-15 indicate that the model of exponentially declining SFR + shallower slope IMF (or continuous star formation models) is preferable for both bulge and disk, rather than the model including only old age stars and steeper slope IMF. We emphasize that the models of long term star-forming is preferable not only for disks but also for most of bulges. Note that the same result has been reported in BD01 for disks.

To check the validity of the M/L s, we illustrate the M/L_V vs. M/L_I diagram and the M/L_V vs. M/L_J diagram in figure 16 and 17, respectively. The W94 models of single starburst with Salpeter IMF, the age= 1.5 to 17 Gyr, and $[\text{Fe}/\text{H}] = -2.0$ to 0.5 are plotted in the (a) part of figures 16 and 17. We also illustrate the comparison of the bulge the counterpart disk in the same galaxy in the (b) part of figure 16 and 17. We find that the obtained M/L s for both of bulges and disks agree with the

Table 8. *I* band M/L ratios and halo parameters.

Name (1)	$(M/L_I)_b$ (2)	$\sigma_{(M/L_I)b}$ (3)	$(M/L_I)_d$ (4)	$\sigma_{(M/L_I)d}$ (5)	σ_h (6)	R_h (7)	rms (8)
N 253	21.04:	7.39	1.60	0.33	-	-	18.06
N 891	-	-	-	-	-	-	no fit
N 1068	1.11	0.32	0.74	0.31	-	-	22.42
N 2403	14.00:	6.22	1.42	0.72	109.64	0.28	3.13
N 2841	1.08	0.21	2.59	0.41	745.46	1.93	43.67
N 2903	3.53	1.10	1.48	0.35	151.97	0.23	11.16
N 3031	3.14	0.53	0.97	0.22	118.65	0.15	29.76
N 3079	16.40:	5.02	0.90	0.25	128.75	0.09	20.59
N 3198	0.23:	0.81	1.34	0.44	123.77	0.17	5.67
N 3521	1.69	0.36	1.69	0.46	135.61	0.21	13.64
N 4192	1.87	0.31	1.10	0.26	-	-	32.20
N 4258	6.29	1.65	0.97	0.30	187.18	0.39	24.53
N 4321	4.16	1.50	2.46	0.91	-	-	4.02
N 4535	5.81:	2.83	1.48	0.31	-	-	12.67
N 4536	3.34	0.90	1.80:	0.77	-	-	14.09
N 4548	2.27	0.86	0.75	0.13	-	-	13.18
N 4565	6.82:	1.61	1.14	0.23	84.42	0.40	13.84
N 4569	0.77	0.51	0.97	0.23	-	-	24.08
N 4736	0.89	0.28	1.23	0.72	63.13	0.09	4.41
N 5194	5.68	1.40	2.14	0.50	-	-	48.42
N 5457	17.73:	8.61	3.29:	1.95	-	-	2.79
N 5907	12.62:	4.28	1.28	0.22	120.56	0.30	12.39
N 6946	17.09:	21.16	1.90	0.87	196.40	0.69	6.84
N 7331	1.67	0.35	0.91	0.26	531.05	0.83	14.05

The colons denote unreliable data (see text).

- (1) NGC Number. (2) Bulge M/L at the *I* band. (3) 1σ error of the bulge M/L . (4) Disk M/L at the *I* band.
(5) 1σ error of the disk M/L . (6) Halo velocity dispersion in $10^2[\text{km s}^{-1}]$ unit. (7) Halo core radius [kpc].
(8) Residual in $[\text{km s}^{-1}]$ unit.

model lines of the age sequences, and the bulges are generally older than the counterpart disks in the figure 16 and 17. The ages of bulges and disks are not uniform but widely distributed. It is clear that the variety of M/L values for both bulge and disk is caused mainly by the age rather than by the metallicity. Moreover, the distribution of bulge age is wider than that of disk; some bulges are older and the others are as same as or younger than disks. The age effect would be dominant rather than the metallicity effect and the dust extinction in these figures, however the degeneracy is not entirely solved. At least, these figures show that some bulges have low M/L s and therefore these bulges are young even if the dust extinction or the variety of metallicity also cause the wide distribution of bulge M/L s.

Our result is contrary to the prediction of monolithic collapse model, in which the bulges were formed from the primordial gas with single starburst, thus must be uniformly old. Our result shows that the ages of bulges are distributed widely, however they are generally older than the disks. On the other hand, in the secular evolution scenario the pseudo bulge is formed gradually and include young stars via the secondary star formation in addition to the classical bulge component of old age. Consequently our result suggests that the secular process (formation and evolution) scenario is valid at least for some galaxies.

5.2. Correlation between Morphological Type and M/L

To investigate the bulge evolution with morphology, we illustrate diagrams of Hubble type index versus M/L_I in figure 18 and the bulge-to-total luminosity (B/T) ratios in the *I* band versus M/L_I in figure 19. We find in these figures that the bulge M/L s increase with increasing Hubble type index or decreasing B/T , while the disk M/L s do not correlate with the type or B/T . Unfortunately the bulge M/L of later-type (Sc or later) in figure 18 is lack because the reliable data of bulge M/L do not exist in the later-type. The trend do not change even if the unreliable data are included, however. The trend is more obvious in figure 19 (B/T v.s. M/L diagram) than figure 18 (type index v.s. M/L diagram). We consider that the B/T obtained directly from the decomposition is more accurate than the type index classified by eye. The correlation suggests that bulges of earlier-type spirals (Sab and Sb) are younger than those of later-type spirals (Sbc or later), as Kauffmann (1996) has predicted. We therefore consider that the secondary star formation occurs in bulges of earlier-type spirals rather than those of later-type spirals. Probably the bulge in the galaxy would be the sum of the classical bulge component (formed from the rapid process at high- z) and the pseudo bulge component (formed from the slow process until today). The pseudo bulge

Table 9. J band M/L ratios and halo parameters.

Name	$(M/L_J)_b$	$\sigma_{(M/L_J)_b}$	$(M/L_J)_d$	$\sigma_{(M/L_J)_d}$	σ_h	R_h	rms
(1)	(2)	(3)	(4)	(5)	(6)	(7)	(8)
N 253	2.42:	0.56	0.61	0.10	-	-	21.35
N 891	-	-	-	-	-	-	no fit
N 1808	-	-	-	-	-	-	no fit
N 2841	1.01	0.28	1.18	0.27	347.87	0.71	32.75
N 2903	0.86:	0.14	0.62:	0.12	-	-	23.69
N 3031	1.33	0.23	0.39	0.18	121.84	0.11	26.67
N 3079	1.61:	0.26	0.40	0.08	31.77	0.00	16.72
N 3198	0.25:	0.48	0.51:	0.18	119.37:	0.05:	8.62
N 3521	0.87	0.20	0.62	0.18	131.52	0.13	13.14
N 3628	6.81:	2.16	0.61	0.15	191.25	0.19	22.39
N 4258	0.52:	0.10	0.95:	0.24	178.60:	0.29:	27.18
N 4303	0.98	0.43	0.47	0.29	135.24	0.11	1.33
N 4321	1.35:	0.41	1.41:	0.42	-	-	4.70
N 4535	7.28:	3.05	1.33:	0.25	-	-	12.71
N 4536	-	-	-	-	-	-	no fit
N 4631	0.55:	0.42	1.27	0.28	120.58	0.22	13.16
N 4736	0.15:	0.05	0.78:	0.22	110.58:	0.07:	9.19
N 5907	3.43:	0.68	0.43	0.07	149.43	0.25	17.47
N 6946	5.15:	1.82	1.22	0.53	155.43	0.36	4.15
N 7331	0.79	0.20	0.37	0.14	665.95	1.09	13.47

The colons denote unreliable data (see text).

(1) NGC Number. (2) Bulge M/L at the J band. (3) 1σ error of the bulge M/L . (4) Disk M/L at the J band.

(5) 1σ error of the disk M/L . (6) Halo velocity dispersion in $10^2[\text{km s}^{-1}]$ unit. (7) Halo core radius [kpc].

(8) Residual in $[\text{km s}^{-1}]$ unit.

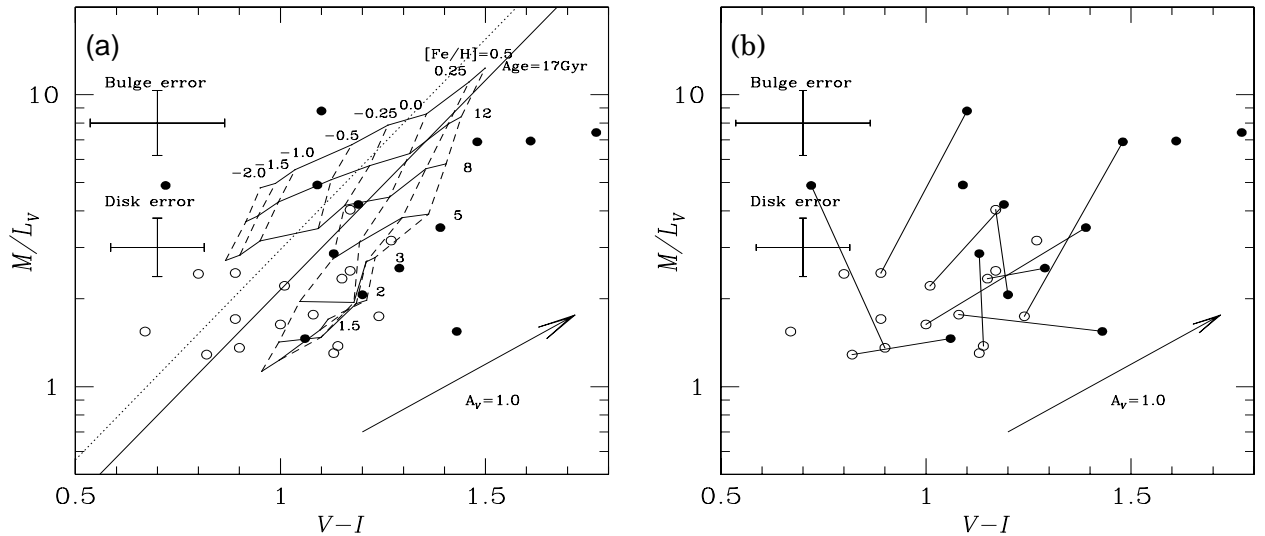


Fig. 13. The color- M/L diagram in the V band. The filled and open circles represent the bulges and the disks, respectively. Only reliable data are plotted. The error bars represent the typical errors for bulge and disk. (a) : Comparison with the models. The different models are as follows: GISSEL96 with Scalo IMF (solid line), with Salpeter IMF (dotted line). The models of W94 of the same age are connected by solid lines, while the models of the same metallicity are connected by dashed lines. (b) : Comparison the bulge with the counterpart disk for the same galaxy, by connecting with solid lines. Only reliable data for both the bulge and disk in the same galaxy are connected.

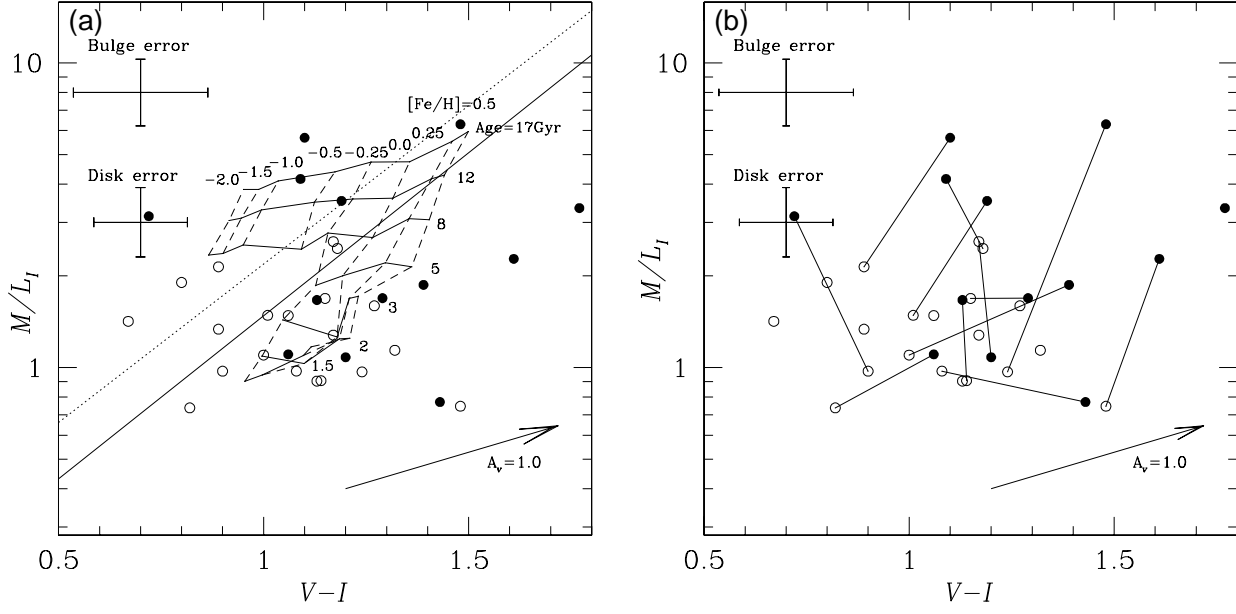


Fig. 14. The color- M/L of I band diagram. The symbols are the same as for figure 13.

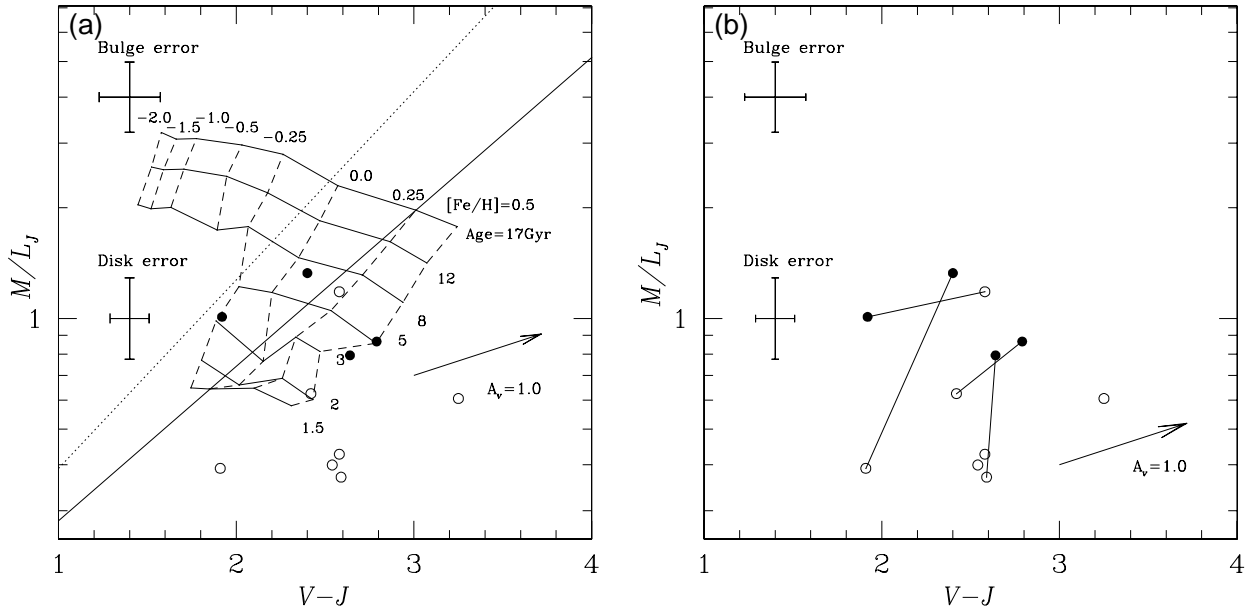


Fig. 15. The color- M/L of J band diagram. The symbols are the same as for figure 13.

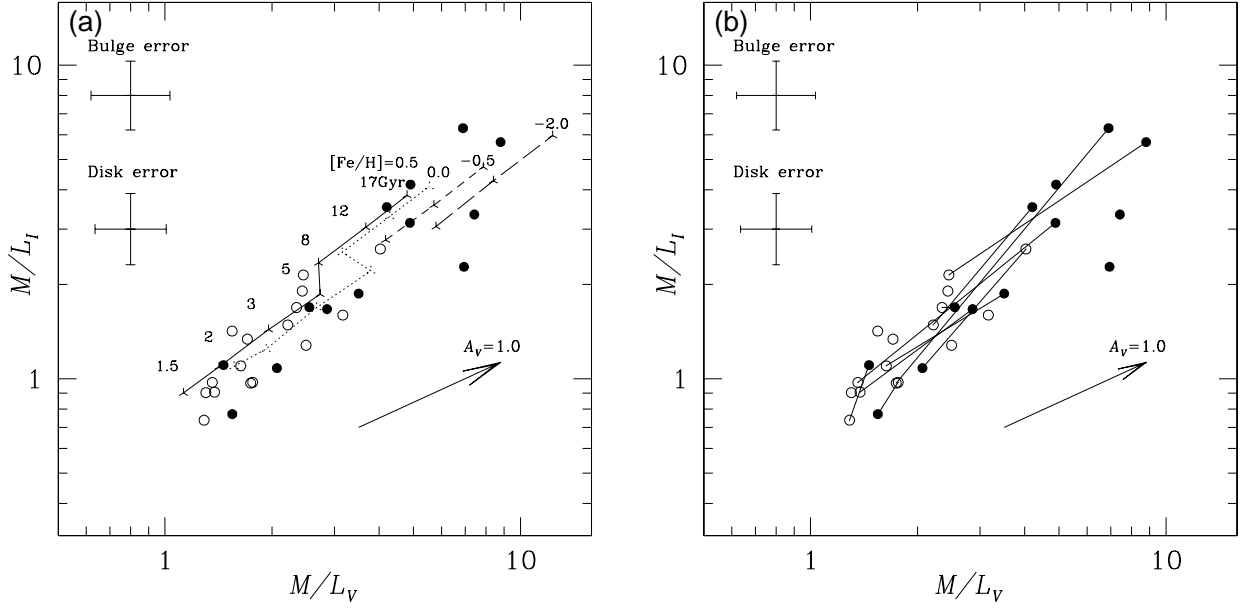


Fig. 16. The M/L_V - M/L_I diagram. The filled and open circles represent the bulges and the disks, respectively. Only reliable data are plotted. (a) : Comparison with models. The models of W94 of $[Fe/H]=0.5, 0.0, -0.5$ and -2.0 are shown. The dots represent ages of 1.5, 2, 3, 5, 8, 12 and 17 Gyr. (b) : Comparison the bulge with the counterpart disk for the same galaxy, by connecting with solid lines. Only reliable data for both the bulge and disk in the same galaxy are connected.

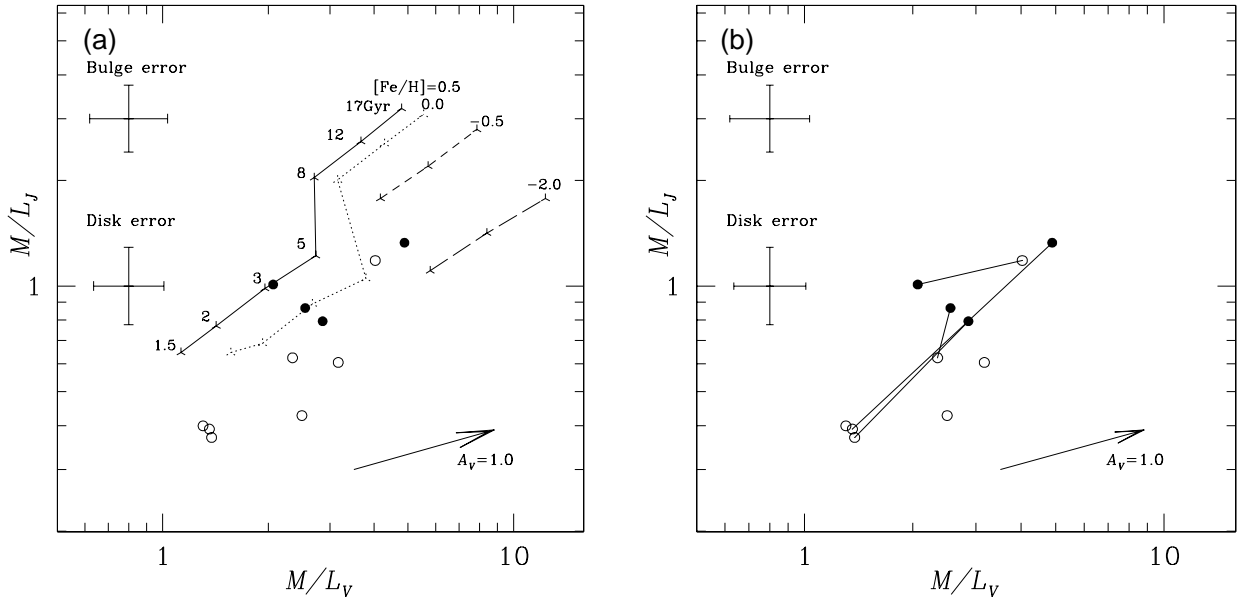


Fig. 17. The M/L_V - M/L_J diagram. The symbols are the same as for figure 16.

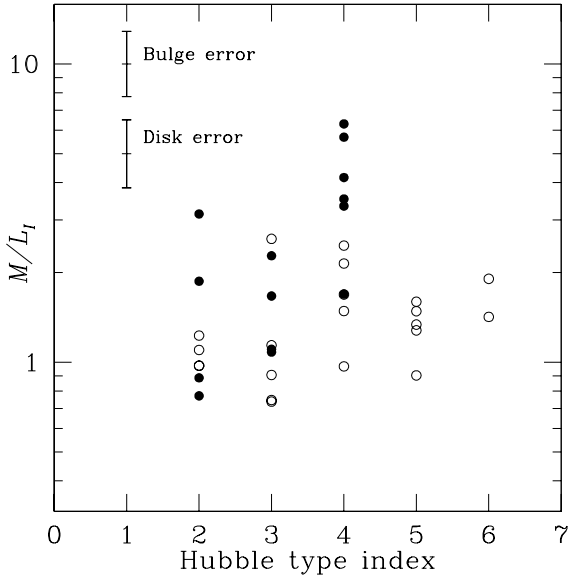


Fig. 18. The Hubble type index versus M/L in the I band. The filled and open circles denote the bulges and the disks, respectively. Only reliable data are plotted.

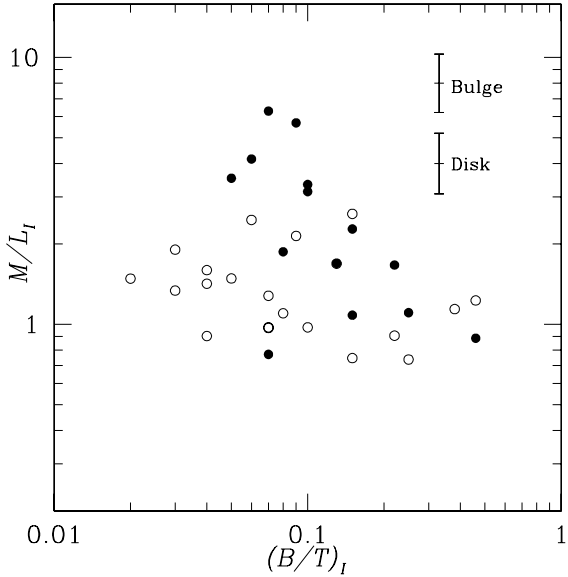


Fig. 19. The B/T versus M/L in the I band. The symbols are the same as for figure 18. Only reliable data are plotted.

component would be dominant in the earlier-type spirals while the classical bulge component would be dominant in the later-type spirals. However, since the number of M/L sample is small and limited to the type of Sab-Sbc, further observation is necessary to confirm the correlation.

5.3. Correlation between Bulge Parameters and Disk Parameters

Previous works (e.g., de Jong 1996b, Möllenhoff, Heidt 2001, MacArthur, Courteau 2003, Hunt et al. 2004) reported that there are some correlations between the structural parameters of bulge and disk, and considered the correlation as the evidence of secular evolution of bulge. We illustrate the disk central luminosity μ_0 versus the bulge effective luminosity μ_e in figure 20. Assuming that the bulges are formed separately from the disks as monolithic collapse scenario predicts, no correlation between the bulges and the disks should be found. The bulge effective luminosity correlates with the disk central luminosity in figure 20, however. In addition, most of earlier type ($T=2, 3$) galaxies locate in the upper-right of the diagram, while later type galaxies ($T=4, 5, 6$) galaxies locate in the lower-left. That is, the early type spirals have generally brighter μ_e and μ_0 than the late type spirals. Figure 21 shows the disk total luminosity versus the bulge total luminosity. The same tendency as for figure 20 is seen in figure 21. This result agrees with de Jong (1996b).

We also confirm the correlation between scale lengths of bulge and disk, which is reported in previous works. The bulge scale length r_{hb} is transformed from the bulge effective radius r_e using the equation $r_{hb} = r_e / (1.9986/\beta - 0.327)^{1/\beta}$ (e.g., Moriondo et al. 1998a, Möllenhoff, Heidt 2001). Figure 22 shows the comparison between the bulge scale length r_{hb} and that of disk r_{hd} for the I band. Although the dispersion is large, the r_{hb} is roughly proportional to the r_{hd} and r_{hb}/r_{hd} is independent of the Hubble type. We obtain the ratio $r_{hb}/r_{hd} = 0.08 \pm 0.05$. Our result agrees with the previous works. Courteau, de Jong, Broeils (1996) reported that it is 0.09 ± 0.04 for the galaxies of de Jong (1996b), and MacArthur, Courteau (2003) reported that it is 0.13 ± 0.06 for 121 late-type galaxies. Courteau, de Jong, Broeils (1996) claimed that the constant r_{hb}/r_{hd} indicates the signature of secular formation because a numerical simulation of disk galaxies evolve toward a double exponential profile with a typical ratio between bulge and disk scale length near 0.1. However, the bulge scale length r_{hb} depends on the value of β . Being adopted $\beta = 1/4$ (de Vaucouleurs' law) instead of $\beta = 1$, the ratio of bulge/disk radii is significantly changed, as Moriondo et al. (1998a), Graham (2001) and Hunt et al. (2004) have pointed out. Hunt et al. (2004) reported that the tight correlation is found for $\beta = 1/3$ and $\beta = 1/4$ bulges and disks, but it disappeared for $\beta = 1$ bulges and disks. The adopted β is nearly 1 for many galaxies in this paper as well as de Jong (1996b), hence the similar results as Courteau, de Jong, Broeils (1996) would be obtained.

Moreover, we investigate the color-magnitude relation in figure 23. If a tight correlation is found, the system should have an age and a metallicity similar to elliptical galaxies. There is no tight correlation in the figure for both bulges and disks. This implies that the age of bulge is not uniform. Although the dispersion is large, the brighter bulges tend to have slightly bluer than the fainter bulges,

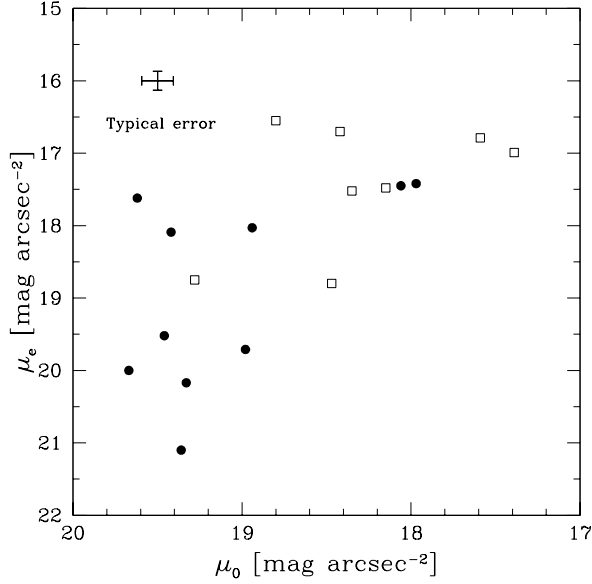


Fig. 20. The comparison of disk μ_0 with bulge μ_e for I band. The squares and circles represent early ($T \leq 3$) and late ($T \geq 4$) type galaxies, respectively.

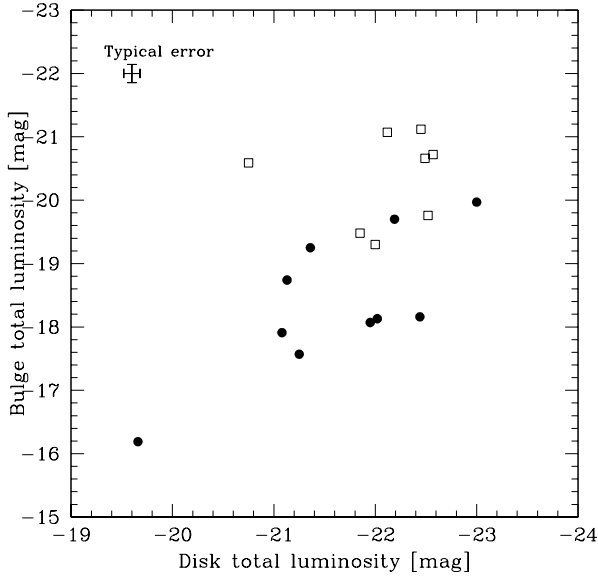


Fig. 21. The comparison of disk total luminosity with bulge total luminosity for I band in absolute magnitude unit. The squares and circles represent early ($T \leq 3$) and late ($T \geq 4$) type galaxies, respectively. The error bar does not include the error of estimating distance.

i.e., the brighter bulges would include young stars. The result also implies the secondary star formation in the bulges of earlier-type spirals.

5.4. Comparison with The Previous Researches

The surface brightness for some galaxies have been decomposed into bulge and disk in previous works. We

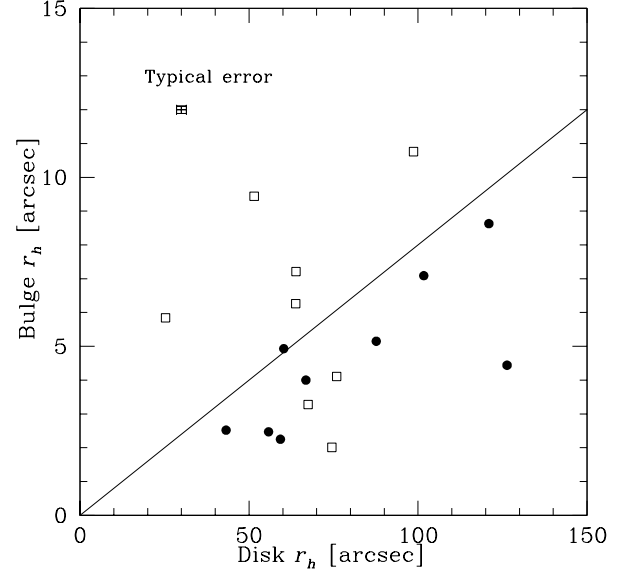


Fig. 22. The comparison of scale lengths between bulge and disk in I band. The open squares and filled circles represent early ($T \leq 3$) and late ($T \geq 4$) type galaxies, respectively. The solid line shows $r_{hb} = 0.08 r_{hd}$.

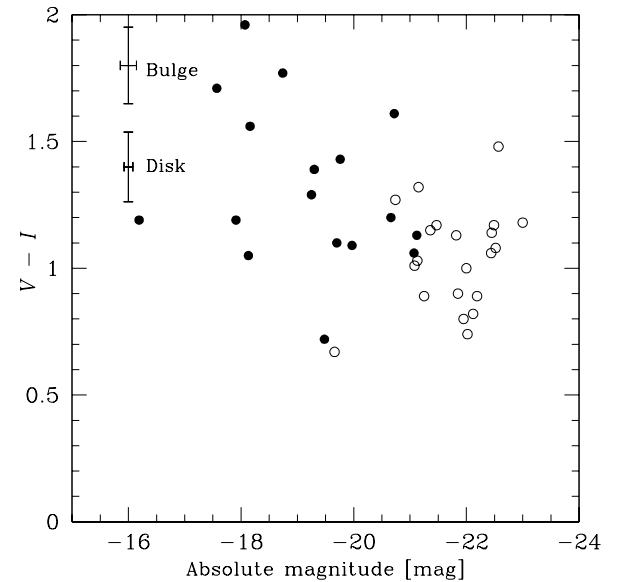


Fig. 23. The color-magnitude diagram. The $V - I$ color and I band absolute magnitude of bulge and disk are shown. The filled and open circles represent the bulges and the disks, respectively. The error bar does not include the error of estimating distance.

compare the surface brightness parameters of the present study with those of previous works. NGC 2841 and NGC 3521 are decomposed by Möllenhoff (2004), NGC 4321 is decomposed by de Jong (1996a), and NGC 7331 is decomposed by Bottema (1999) at the I band. Note that various units of parameters for bulge are used in these papers; μ_e (effective magnitude) or μ_0 (central magnitude), r_e (effective radius) or r_h (scale length), and kpc unit or arcsec unit. To avoid confusion, the scale length r_h in arcsec unit and the central magnitude μ_0 for bulge are used in this section instead of the effective radius r_e and effective magnitude μ_e . Figure 24 shows the comparison for the parameters at the I band.

The disk parameters of the present paper are roughly consistent with those of previous works in (b) and (d) of figure 24. However, the bulge parameters are inconsistent except for NGC 4321. We consider that the adopted bulge index $\beta = 1/n$ strongly affects the values of structural parameters of bulge and therefore causes the disagreement. In fact, NGC 4321 bulge is fitted with exponential ($\beta = 1$) model in both de Jong (1996a) and this study, and the values of parameters are roughly consistent. The β is 0.25 for the bulges of NGC 2841 and NGC 7331, and is 0.74 for NGC 3521 bulge in previous works, while the β is 1.0 for the bulges of NGC 2841 and NGC 7331 and is 0.67 for NGC 3521 bulge in this study. Baggett, Baggett, Anderson (1998) also present the bulge/disk parameters for 17 galaxies in Table 4 of this paper. We have also compared with their results, but the results are generally inconsistent. We consider the inconsistent is due to the adopted β value; Baggett, Baggett, Anderson (1998) have adopted the $\beta = 1/4$ for all galaxies while we fit mainly with $\beta = 1$.

The disk M/L s in the present study ($M/L_V = 2.0 \pm 0.7$, $M/L_I = 1.4 \pm 0.5$, $M/L_J = 0.7 \pm 0.3$) are somewhat lower than the values of previous researches (e.g., Moriondo, Giovanardi, Hunt 1998b; Palunas, Willimas 2000). The lower M/L s of this paper would be caused by the following two reasons. The difference of assumed distances changes M/L because it is inversely proportional to the distance. In this paper, the distances for 13 galaxies in table 2 are derived from the Cepheid observation. Those for other 15 galaxies are cited from Tully (1988) with $H_0 = 75 \text{ km s}^{-1} \text{ Mpc}^{-1}$. On the other hand, Moriondo, Giovanardi, Hunt (1998b) used the distances derived with $H_0 = 50 \text{ km s}^{-1} \text{ Mpc}^{-1}$. If we adopt $H_0 = 72 \text{ km s}^{-1} \text{ Mpc}^{-1}$ (Freedman et al. 2001), the average of their disk M/L_J ratios is about 1.1 (originally 1.6). Thus the discrepancy is reduced, however the disk $M/L_J = 0.7 \pm 0.3$ in the present study is still lower than Moriondo, Giovanardi, Hunt (1998b). The other reason of discrepancy would be the correction of systematic error of the maximum disk solution discussed in section 3.4. The corrected value of disk M/L is reduced by a factor of 0.9-1.0 compared with the original value.

The bulge M/L s in the present study are 4.5 ± 2.3 , 2.7 ± 1.7 and 1.0 ± 0.2 in V , I and J band, respectively. Kent (1986) reported that the average bulge M/L in r band (an intermediate band between V and I) is 4.6 using

optical emission line rotation curves and $H_0 = 50$, which is 3.2 using $H_0 = 72$. In addition, using H I rotation curves, Kent (1987) reported that it is 2.9 ($H_0 = 72$). Although the rotation curves used in Kent (1986) were not the CO observation, these bulge M/L s agree roughly with our result. Moreover Moriondo, Giovanardi, Hunt (1998b) reported that the average bulge M/L in J band is 1.1 ($H_0 = 50$), which is 0.76 using $H_0 = 72$. It is also roughly consistent with the bulge $M/L_J = 1.0 \pm 0.2$ in this study within 1 sigma. They claimed that the bulges of early-type (Sa-Sb) are younger than disks, however the $H\alpha$ rotation curves used in their studies are softened near the galactic center. The CO rotation curves give more rapidly rotation curves than the $H\alpha$ rotation curves near the galactic center, hence we tend to obtain the higher bulge M/L than the previous studies. The other reason would be the correction for the systematic error of M/L ; the corrected value of bulge M/L is about factor of 1.0-1.3 higher than that of original value. If the correction is not applied, the bulge M/L in this paper is reduced by a factor of 0.7-1.0, and the discrepancy between our result and Moriondo, Giovanardi, Hunt (1998b) would be reduced.

Using color-color diagram, Peletier et al. (1999) reported that the bulge colors of early-type (S0-Sb) are uniformly red and thus the ages are as old as most of elliptical galaxies in cluster. However, W94 claimed that the colors are not sensitive to age except for extremely young case ($< 2 \text{ Gyr}$) and are affected by the age-metallicity degeneracy. Our bulge $V - I$ is 1.33 ± 0.30 , which is somewhat redder than disk $V - I = 1.05 \pm 0.20$. Therefore our result is not inconsistent with the report of Peletier et al. (1999) for the bulge color. The M/L has the advantage of being more sensitive to age than colors. Hence the color- M/L diagram reveals the spread of age for bulges rather than the color-color diagram. Our result shows that the bulge age is not uniform and that the bulges of earlier-type galaxies are younger than those of later-type galaxies and nearly as same age as the disks. However, the type of our bulge M/L data is only from Sab to Sbc. Further observation for S0-Sa and Sc-Sd galaxies are needed to confirm the formation of bulges.

6. Conclusion

Using optical and near-infrared (V , I and J) band images, we decomposed the surface brightness of galaxies into bulge and disk components. We obtained the M/L s for bulges and disks with CO rotation curves for the inner part of galaxies. We compared the colors and the M/L s with those of galaxy formation models. We found the correlation between the colors and the M/L s for bulges and disks, and that the correlation between B/T and the M/L . Our results are generally consistent with galaxy formation models of slowly star-forming system; with an exponentially declining SFR and shallow slope IMF (ex. Scalo IMF). The exponentially declining SFR taken from BD01 is suitable not only for disks but also for bulges. Moreover we found that the bulge M/L s of earlier-type spirals are lower than those of later-type

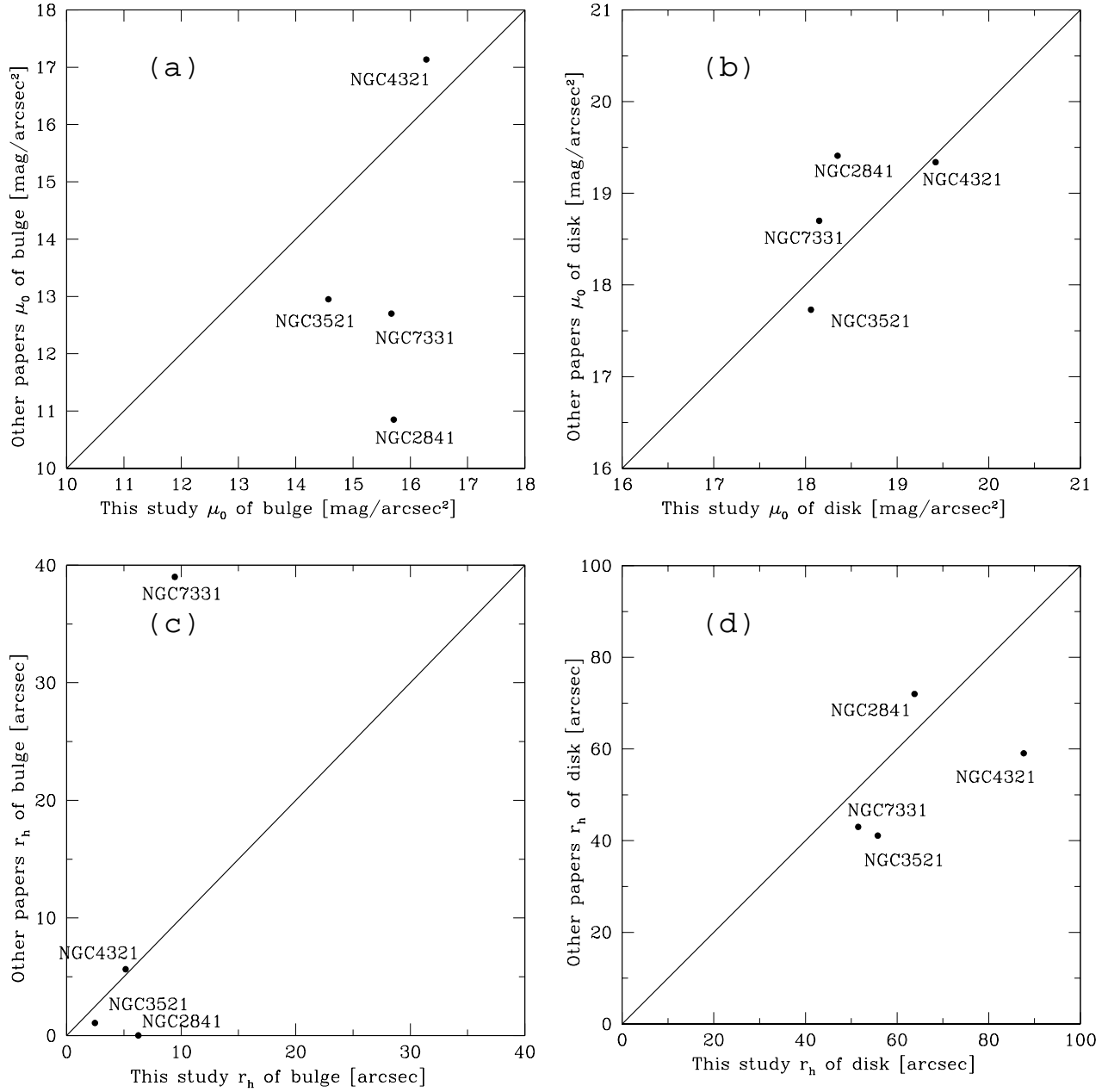


Fig. 24. The comparison of surface brightness parameters in this study with the previous papers. (a) central magnitude of bulge. (b) scale length of bulge. (c) central magnitude of disk. (d) scale length of disk. The solid lines in each panel show the equality.

spirals. These facts suggest that the luminosity-weighted average ages of the bulges in earlier-type galaxies are younger than those of later-type galaxies. Moreover, we confirmed the correlations between bulge parameters and disk parameters as previous authors reported. In addition there is no tight correlation between the colors and magnitudes for both bulges and disks. These results suggest that the bulges of earlier-type galaxies would not be the classical bulge but be the pseudo bulge as the secular formation scenarios predict.

We would like to thank an anonymous referee for careful reading of the manuscript and valuable comment on this work. We wish to thank Shin-ichi Ichikawa, Fumiaki Nakata and Yoshihiko Yamada of Astronomy Data Center of National Astronomical Observatory of Japan for useful comment. We also wish to thank Yumiko Tanaka of Kiso Observatory for obtaining KONIC data. This work is based on data collected at Kiso observatory (University of Tokyo) and obtained from the SMOKA, which is operated by the Astronomy Data Center, National Astronomical Observatory of Japan. Data analysis was in part carried out on "sb" computer system operated by the Astronomy Data Center of the National Astronomical Observatory of Japan. This work has been supported in part by the Grant-in-Aid for Scientific Research 11554005 and 14340059 of the Ministry of Education, Science, Culture, and Sports in Japan.

References

- Aguerri, J. A., Balcells, M., & Peletier, R. F. 2001, *A&A*, 367, 428
- Andredakis, Y. C., & Sanders, R. H. 1994, *MNRAS*, 267, 283
- Andredakis, Y. C., Peletier, R. F., & Sanders, R. H. 1995, *MNRAS*, 275, 874
- Arimoto, N., & Yoshii, Y. 1987, *A&A*, 173, 23
- Baggett, W. E., Baggett, S. M., & Anderson, K. S. J. 1998, *AJ*, 116, 1626
- Barnaby, D., & Thronson, H. A., Jr. 1994, *AJ*, 107, 1717
- Balcells, M., Graham, A. W., Domínguez-Palmero, L., & Peletier, R. F. 2003, *ApJL*, 582, 79
- Bell, E. F., & de Jong, R. S. 2001, *ApJ*, 550, 212
- Binney, J., & Tremaine, S. 1987, *Galactic Dynamics*, Princeton University Press (Princeton, New Jersey)
- Bosma, A. 1981, *AJ*, 86, 1791
- Bottema, R. 1999, *A&A*, 348, 77
- Bruzual, G., & Charlot, S. 1993, *ApJ*, 405, 538
- Byun, Y. I., & Freeman, K. C. 1995, *ApJ*, 448, 563
- Caon, N., Capaccioni, M., & D'Onofrio, M. 1993, *MNRAS*, 265, 1013
- Carignan, C., & Freeman, K. C. 1985, *ApJ*, 294, 494
- Courteau, S., de Jong, R. S., & Broeils, A. H. 1996, *ApJL*, 457, 73
- de Jong, R. S. 1996a, *A&AS*, 118, 557
- de Jong, R. S. 1996b, *A&A*, 313, 45
- de Vaucouleurs, G. 1953, *MNRAS*, 113, 134
- de Vaucouleurs, A., & Longo, G. 1988, *Catalogue of Visual and Infrared Photometry of Galaxies from 0.5 μ m to 10 μ m (1961-1985)* (Austin: The University of Texas)
- de Vaucouleurs, G., de Vaucouleurs, A., Corwin, H. G., Jr., Buta, R. J., Paturel, G., & Fouqué, P. 1991, *Third Reference Catalogue of Bright Galaxies* (New York: Springer) (RC3)
- Eggen, O. J., Lynden-Bell, D., & Sandage, A. R. 1962, *ApJ*, 136, 748
- Ferrarese, L., et al. 1996, *ApJ*, 475, 853
- Fillmore, J. A., Boroson, T. A., & Dressler, A. 1986, *ApJ*, 302, 208
- Freeman, K. C. 1970, *ApJ*, 160, 811
- Freedman, W. L., & Madore, B. F. 1988, *ApJ*, 332, 63
- Freedman, W. L., et al. 1994, *ApJ*, 427, 628
- Freedman, W. L., et al. 2001, *ApJ*, 553, 47
- Graham, A. W. 2001, *ApJ*, 121, 820
- Greenhill, L. J., Gwinn, C. J., Antonucci, R., & Barvainis, R. 1996, *ApJ*, 472, 21
- Hughes, S. M. G., et al. 1998, *ApJ*, 501, 32
- Hunt, L. K., Pierini, D., & Giovanardi, C. 2004, *A&A*, 414, 905
- Ichikawa, S., Okamura, S., Watanabe, M., Hamabe, M., Aoki, T., & Kodaira, K. 1987, *Ann. Tokyo Astron. Obs.*, 21, 285
- Itoh, N., Yanagisawa, K., Ichikawa, T., Tarusawa, K., & Katata, N. 1995, *SPIE*, 2552, 430
- Kauffmann, G. 1996, *MNRAS*, 281, 487
- Kelson, D. D., et al. 1996, *ApJ*, 463, 26
- Kelson, D. D., et al. 1999, *ApJ*, 514, 614
- Kent, S. M. 1986, *AJ*, 91, 1301
- Kent, S. M. 1987, *AJ*, 93, 816
- Kent, S. M. 1988, *AJ*, 96, 514
- Kodama, T., & Arimoto, N. 1997, *A&A*, 320, 41
- Kormendy, J. 1979, *ApJ*, 227, 714
- Kormendy, J., & Kennicutt, R. C., Jr. 2004, *ARA&A*, 42, 603
- Laurikainen, E., Salo, H., Buta, R., & Knapen, J. H. 2007, *MNRAS*, 381, 401
- Leitherer, C., et al. 1996, *PASP*, 108, 996
- MacArthur, L. M., & Courteau, S. 2003, *ApJ*, 582, 689
- Macri, L. M., Stetson, P. B., Bothun, G. D., Freedman, W. L., Garnavich, P. M., Jha, S., Madore, B. F., & Richmond, M. W. 2001, *ApJ*, 559, 243
- Moffat, A. J. J. 1969, *A&A*, 3, 455
- Möllenhoff, C. & Heidt, J. 2001, *A&A*, 368, 16
- Möllenhoff, C. 2004, *A&A*, 415, 63
- Moriondo, G., Giovanardi, C., & Hunt, L. K. 1998a, *A&AS*, 130, 81
- Moriondo, G., Giovanardi, C., & Hunt, L. K. 1998b, *A&A*, 339, 409
- Newman, J. A., Ferrarese, L., Stetson, P. B., Maoz, E., Zepf, S. E., Davis, M., Freedman, W. L., & Madore, B. F. 2001, *ApJ*, 553, 562
- Norman, C., Sellwood, J. A., & Hasan, H. 1996, *ApJ*, 462, 114
- Palunas, P., & Willimas, T. B. 2000, *AJ*, 120, 2884
- Peletier, R. F., Balcells, M., Davies, R. L., Andredakis, Y., Vazdekis, A., Burkert, A., & Prada, F. 1999, *MNRAS*, 310, 703
- Press, W. H., Flannery, B. P., Teukolsky, S. A., & Vetterling, W. T. 1988, *Numerical Recipes in C*, (Cambridge and New York: Cambridge University Press)
- Portinari, L., Sommer-Larsen, J., & Tantalo, R. 2004, *MNRAS*, 347, 691
- Rubin, V. C., Burstein, D., Ford, W. K., Jr., & Thonnard, N. 1985, *ApJ*, 289, 81
- Rubin, V. C., Kenney, J. D. P., & Young, J. S. 1997, *AJ*, 113, 1250

- Salpeter, E. E. 1955, ApJ, 121, 161
- Salucci, P., Ratnam, C., Monaco, P., & Danese, L. 2000, MNRAS, 317, 488
- Scalo, J. M. 1986, Fund. Cosmic Phys., 11, 1
- Schlegel, D. J., Finkbeiner, D. P., & Davis, M. 1998, ApJ, 500, 525
- Seigar, M. S., & James, P. A. 1998, MNRAS, 299, 672
- Sérsic, J. L. 1968, Atlas de galaxias australes, (Cordoba, Observatorio Astronomica)
- Sofue, Y. 1996, ApJ, 458, 120
- Sofue, Y. 1997, PASJ, 49, 17
- Sofue, Y., Tutui, Y., Honma, M., & Tomita, A. 1997, AJ, 114, 2428
- Sofue, Y., Koda, J., Nakanishi, H., & Onodera, S. 2003, PASJ, 55, 59
- Takamiya, T., Sofue, Y., ApJ, 534,670
- Tully, B. R. 1988, Nearby Galaxies Catalog, (Cambridge and New York: Cambridge University Press)
- van Albada, T. S., Bahcall, J. N., Begeman, K., & Sancisi, R. 1985, ApJ, 295, 305
- Worthey, G. 1994, ApJS, 95, 107
- Zhang, X. 1999, ApJ, 518, 613